Lightning flash rate and chemistry simulation of tropical island convection using a cloud-resolved model

Kristin A. Cummings

Department of Atmospheric and Oceanic Science

University of Maryland

College Park, MD 20742

Submitted as M.S. Scholarly Paper

May 2013

Advisor: Dr. Kenneth E. Pickering

A portion of this scholarly paper has been published as:

Cummings, K. A., et al., Cloud-resolving chemistry simulation of a Hector thunderstorm, *Atmos. Chem. Phys.*, 13, 2757-2777, 2013.

Abstract

Cloud chemistry simulations were performed for a Hector thunderstorm observed on 16 November 2005 during the SCOUT-O3/ACTIVE campaigns based in Darwin, Australia, with the primary objectives of testing flash rate parameterization schemes (FRPSs) and estimating the average NO production per lightning flash in this unique storm type, which occurred in a tropical island environment. The 3-D WRF-Aqueous Chemistry (WRF-AqChem) model is used for these calculations and contains the WRF nonhydrostatic cloud-resolving model with online gas- and aqueous-phase chemistry and a lightning-NO_x (LNO_x) production algorithm. The model was run with observed flashes and with the use of six FRPSs. The model was initialized by inducing convection with an idealized morning sounding and sensible heat source, and initial condition chemical profiles from merged aircraft observations in undisturbed air. Many features of the idealized model storm, such as storm size and peak radar reflectivity, were similar to the observed storm. Tracer species, such as CO, used to evaluate convective transport in the simulated storm found vertical motion from the boundary layer to the anvil region was well represented in the model, with a small overestimate of enhanced CO at anvil altitudes. The lightning detection network (LINET) provided lightning flash data for the model and a lightning placement scheme injected the resulting NO into the simulated cloud. A lightning NO production scenario of 500 moles $flash^{-1}$ for both CG and IC flashes yielded anvil NO_x mixing ratios that compared well with aircraft observations and were also similar to those deduced for several convective modeling analyses in the midlatitudes and subtropics. However, these NO production values were larger than most estimates for tropical thunderstorms and given several uncertainties, LNO_x production may have been as large as 600 moles $flash^{-1}$. Approximately 85% of the simulated LNO_x mass was located above 7 km in the later stages of the storm, which

was greater than amounts found for subtropical and midlatitude convection. Generally, maximum vertical velocity and cloud top height were good predictors of the observed flash rate trend and the associated chemistry within the storm cloud, after scaling factors were applied to each FRPS. Modeled upper tropospheric NO_2 partial columns were also considerably greater than most satellite observations of tropical marine convective events, as tropical island convection, such as Hector, is more vigorous and more productive of LNO_x. Additional research is needed to investigate whether LNO_x production per flash increases in storms with greater wind shear, such as this Hector storm, which showed significant variation in wind direction with altitude.

1 Introduction

Tropospheric ozone (O_3) plays important roles in determining the oxidizing capacity of the atmosphere and in affecting climate forcing. Nitrogen oxides ($NO_x = NO + NO_2$) are the most critical precursor gases for photochemical O_3 formation. NO_x also influences the HO_x radicals ($HO_x = HO + HO_2$), which are major oxidants of numerous chemical species. Fossil fuel combustion, biomass burning, microbial activity in soils, and lightning are considered the four major sources of tropospheric NO_x. Lightning generates less NO_x than anthropogenic sources, but does so mainly in the middle and upper troposphere where NO_x is longer-lived and more efficient at producing O_3 than in the boundary layer where much of the anthropogenic NO_x is emitted. The best estimate of the global lightning-generated NO_x (LNO_x) source is 5 ± 3 Tg N yr^{-1} (Schumann and Huntrieser, 2007). The uncertainty in the source strength is due to both an uncertainty in the total number of flashes globally and the amount of NO_x per flash or per meter of flash length. Satellite observations of lightning have narrowed the uncertainty in the global flash rate, but the NO_x production issue remains uncertain. This issue is further complicated because cloud-to-ground (CG) flashes and intracloud (IC) flashes may produce different amounts of NO_x. Schumann and Huntrieser (2007) provide a detailed review of three decades of research on the global LNO_x source rate.

One method used in estimating NO_x production per flash is through application of cloud-resolving models. Most of these simulations, to date, have focused on midlatitude and subtropical convective systems. Midlatitude convection primarily occurs in the $35^o – 45^o$ latitude belt in both hemispheres, often associated with synoptic-scale weather systems. Subtropical and tropical convection is found closer to the equator, away from the influence of midlatitude systems, and is differentiated based on development within air masses of lower and higher

equivalent potential temperatures, respectively (Huntrieser et al., 2007). Attention is now turning to data from several atmospheric chemistry field programs recently conducted in tropical convective environments. We focus here on the simulation of a Hector thunderstorm observed on 16 November 2005 during the Stratospheric-Climate Links with Emphasis on the Upper Troposphere and Lower Stratosphere (SCOUT-O3; Brunner et al., 2009) and Aerosol and Chemical Transport in Tropical Convection (ACTIVE; Vaughan et al., 2008) field experiments based in Darwin, Australia. The name Hector is given to the very deep convective storms which develop over the Tiwi Islands offshore from Darwin, particularly during the transition season (November-December) prior to the monsoon onset. These two field experiments incorporated detailed lightning observations and atmospheric chemical sampling of the anvil by aircraft. This allowed for evaluation of model flash rate parameterization schemes (FRPSs) and estimation of LNO_x production from model calculations constrained by the anvil observations.

Deep convection has important effects on atmospheric chemistry, which include the rapid redistribution of chemical constituents from the boundary layer to the upper troposphere (Chatfield and Crutzen, 1984; Dickerson et al., 1987). Here lower temperatures slow reaction rates, which generally allows chemical species in the upper troposphere to have longer lifetimes and therefore be transported globally. Chemical consequences of the transport of boundary layer air to the upper troposphere can include changes in water vapor that lead to changes in HO_x, as well as changes in O_3 (Pickering et al., 1990, 1992) and precursors. Over most of the tropics, low mixing ratios of O_3 and NO_x are transported to the tropical tropopause layer (Pickering et al., 1993; Wang and Prinn, 2000; Salzmann et al., 2008) except over polluted areas, such as urban centers and biomass burning regions. Other chemical consequences include changes in aerosol concentrations and the aforementioned LNO_x production and transport. Thunderstorms inject

NO_x from lightning into the middle and upper troposphere. Over relatively unpolluted regions of the tropics, LNO_x can be the dominant chemical effect of deep convection. Along with enhanced HO_x in the upper troposphere, LNO_x leads to efficient O_3 production in this layer of up to several ppbv per day (DeCaria et al., 2005). Ozone, the third most important greenhouse gas, is most effective in this role in the upper troposphere and lower stratosphere (IPCC, 2007). Therefore, better knowledge of LNO_x production is important for the understanding of climate forcing. Cloud-resolving models with chemistry, after evaluation with field observations, can be used to better understand convective transport processes and LNO_x production. Cloud-scale models are valuable because they can simulate the transport and distribution of NO_x and its contribution to photochemistry at scales directly comparable to airborne observations in thunderstorms (Schumann and Huntrieser, 2007).

This study provides the first analysis of a cloud-resolved LNO_x simulation of deep convection in the tropics for which detailed lightning flash data and anvil NO_x measurements are available. The primary objectives are to test FRPSs and estimate the average production of NO per lightning flash in a tropical environment. However, tropical island convection, like Hector thunderstorms, may not be representative of other types of convection found in the tropics. Section 2 reviews selected LNO_x cloud-resolved simulations, analysis of results from airborne tropical LNO_x experiments, and numerical modeling studies of tropical thunderstorms over the Maritime Continent. Section 3 describes the ground-based and aircraft observations of the Hector thunderstorm. Section 4 provides a description of the Weather Research and Forecasting Aqueous Chemistry (WRF-AqChem) model and initialization data. Section 5 compares the meteorological and chemical features of the observed and simulated thunderstorm, including the

incorporation of FRPSs into the model, and Sect. 6 presents the conclusions from our cloud-resolved tropical island convection simulation.

2 Background

2.1 Lightning-Produced NO_x in Cloud-Resolving Models

To simulate LNO_x production, the flash rate, type of flash, NO source location, and amount of NO produced must be represented. Cloud-resolved models have previously been used to forecast total (CG and IC) lightning flashes using relationships between ice-phase hydrometeors and lightning. McCaul et al. (2009) developed several methods for determining flash rates using graupel and vertically integrated ice based on selected convective events over Northern Alabama. While the strengths of each method capture different aspects of the lightning activity, such as temporal variability and areal coverage, respectively, it was determined that a combination of the two methods better predicted the flash rates over their case study region.

Previous research has also investigated correlations between lightning and non-hydrometeor parameters. These parameters include maximum vertical velocity, cloud top height, and updraft volume. Barthe et al. (2010) incorporated six FRPSs based on storm parameters that are already available in models. Their research differs from previous work because it was the first time field experiment observations were used to create flash rate-storm parameter relationships, which were tested in a model. The modeled storm parameters were then adjusted within the flash rate equations, based on the relationships between observed and modeled storm parameters for specific thunderstorms. Therefore, flash rates can either be predicted from storm parameters, such as cloud top height, maximum vertical velocity, ice mass fluxes, updraft volume, ice water path, and precipitation ice mass (Price and Rind, 1992; Petersen et al., 2005;

Deierling and Petersen, 2008; Deierling et al., 2008; Barthe et al., 2010) or, to reduce uncertainty, prescribed directly from lightning observations (DeCaria et al., 2005; Ott et al., 2010). Likewise, the flash type can be predicted (Price and Rind, 1993; Pickering et al., 1998; Fehr et al., 2004) or prescribed from observations (DeCaria et al., 2005; Ott et al., 2007, 2010).

The NO source location is generally near the storm core, but can reach several tens of kilometers away (Höller et al., 2009; Kuhlman et al., 2009). In the volumetric approach to parameterizing LNO_x, the DeCaria et al. (2000, 2005) scheme uses the 20 dBZ reflectivity contour as the threshold for the horizontal within-cloud placement of LNO_x. Ott et al. (2007) devised a different LNO_x placement scheme where the resulting NO production tries to better mimic lightning flash channels through a filamentary approach (Barthe and Barth, 2008; Ott et al., 2010). This approach uses a smaller source location, which represents NO production per flash or per meter flash length. NO production per flash can be derived from model results through comparisons with aircraft storm anvil measurements.

Cloud-scale simulations have used various models to estimate NO production per flash and the P_{IC}/P_{CG} ratio, where P_{IC} and P_{CG} are the mean NO production per IC and CG flash, respectively. Table 1 provides a list of the model types, as well as the LNO_x production results from each cloud-resolved simulation. For all simulated storms, the LNO_x was compared against aircraft NO_x observations in the anvils to deduce P_{IC} and P_{CG}. With the cloud-resolved two-dimensional (2-D) Goddard Cumulus Ensemble (GCE) model, Pickering et al. (1998) parameterized the LNO_x source by uniformly distributing individual flashes in the vertical within separate CG and IC lightning regions, where flash rates were predicted based on updraft vertical velocity. Seven convective events from three different regimes (midlatitude continental, tropical continental, and tropical marine) were simulated using the algorithm, and the resulting C-shaped

LNO_x vertical profiles were developed for use in larger scale models. DeCaria et al. (2000, 2005) modified the Pickering et al. (1998) scheme by assuming a more physically realistic non-uniform distribution of lightning channels and using observed IC and CG flash rates. The flash channel vertical modes, as well as NO_x production, followed Gaussian distributions. This general technique has also been used by Ott et al. (2007, 2010) in simulating a series of midlatitude and subtropical thunderstorms. The assumptions that P_{CG} was roughly 460 moles NO $flash^{-1}$ and P_{IC} was 75-100% of P_{CG} (DeCaria et al., 2005) provided the best comparison to the column NO_x mass computed from aircraft observations for the 12 July 1996 Stratosphere-Troposphere Experiment: Radiation, Aerosols and Ozone (STERAO-A) storm. Fehr et al. (2004) and Ott et al. (2007) both studied the production of LNO_x in the midlatitude 21 July European Lightning Nitrogen Oxides Project (EULINOX) storm using different models. Similar results for P_{CG} were obtained and both simulations showed an IC flash produced more LNO_x than a CG flash. Ott et al. (2010) has summarized the LNO_x production results from five 3-D midlatitude and subtropical storm simulations. Mean production per CG flash over the five storms was 500 moles $flash^{-1}$ with a mean P_{IC}/P_{CG} ratio of 0.94.

Explicit electrical schemes have been used by Zhang et al. (2003b) and Barthe et al. (2007) to study LNO_x. A small, isolated, short-lived 19 July 1989 Cooperative Convective Precipitation Experiment (CCOPE) cloud with simple chemistry was simulated using the Storm Electrification Model (SEM) (Zhang et al., 2003a, b). In general, the results indicated the parameterization produced NO mixing ratios comparable to observations with a maximum LNO_x mixing ratio of 35.8 ppbv. Barthe et al. (2007) tested an explicit electrical scheme for LNO_x using the 10 July 1996 STERAO storm. Lightning flash frequency and total path length were the key factors determined by the simulated electrical state of the storm. LNO_x dominated the NO_x

budget in the upper portion of the cells with instantaneous peak mixing ratios exceeding 4 ppbv in accordance with observations. Estimated NO production was 36 moles flash^{-1}.

The cloud-scale model intercomparison performed by Barth et al. (2007b) showed intermodel variability was much larger for simulated NO_x than the chemical tracers, CO and O_3, demonstrating the uncertainty surrounding the NO source placement and its volume within the storm, as each model used a different method. A wide range of LNO_x production rates (36-465 moles flash^{-1}) was noted when six different models were used, yet similar NO_x mixing ratios were obtained in the anvil region. This result, as well as the information gained from using explicit electrification schemes, indicated there is still much to learn about LNO_x production in thunderstorms. One model used in the intercomparison was the WRF-AqChem model by Barth et al. (2007a), which inputs observed flash rates for LNO_x parameterization, similar to DeCaria et al. (2005). The results indicated it was unlikely lightning affects concentrations of HO_x precursors near active convection.

Based on the simulations run by Ott et al. (2010), application of their LNO_x production rates (500 moles flash^{-1}) with the global annual average flash rate of 44 flashes second^{-1} yielded an annual global LNO_x production of about 9 Tg N yr^{-1}, which was significantly larger than the 5 Tg N yr^{-1} estimated by Schumann and Huntrieser (2007). This raises the question as to whether lightning flashes in tropical thunderstorms produce less NO_x on average than flashes in midlatitude or subtropical storms. In this paper, we test whether a NO production scenario of 500 moles flash^{-1} for both IC and CG flashes generates model-simulated NO_x mixing ratios similar to those observed in a Hector thunderstorm.

2.2 LNO_x Production in Tropical Thunderstorms

Wind shear is useful not only as a proxy for ice mass or volume, since it relates to storm dynamics and updraft size (Huntrieser et al., 2008, 2009, 2011), but also for assessing flash length and associated NO_x production in different climate regimes. As lightning activity is physically related to ice mass aloft, it is also associated with environmental shear, as storms grow larger (and contain larger amounts of ice mass) under stronger shear. Huntrieser et al. (2008) hypothesized a tropical flash may produce, on average, less NO than a flash in a midlatitude or subtropical storm because weaker vertical wind shear in the tropics leads to shorter flash channel lengths. If the amount of nitrogen produced by lightning is better correlated with flash channel lengths than the number of strokes, subtropical and midlatitude storms may have a significant impact on global LNO_x even though the majority of global lightning occurs in the tropics.

Several tropical field campaigns have been conducted in an attempt to further investigate regional LNO_x production rates and their impact on global LNO_x. The first aircraft experiment specifically designed to estimate LNO_x production in the tropics was the Biomass Burning and Lightning Experiment (BIBLE-C) based in Darwin, Australia (Koike et al., 2007). On two flights, enhanced upper tropospheric NO_x mixing ratios were attributed to lightning located several hundred kilometers upstream near the Gulf of Carpentaria. Observed lightning data and a LNO_x vertical distribution (Pickering et al., 1998) were used in conjunction with aircraft NO_x observations to estimate LNO_x production rates of 31-73 moles $flash^{-1}$ for one storm and 348-813 moles $flash^{-1}$ in a second system. Based on the Tropical Convection, Cirrus, and Nitrogen Oxides Experiment (TROCCINOX) in Brazil, the LNO_x mass production for tropical thunderstorms was of similar magnitude as that found for one of the BIBLE-C storms (~70

moles flash^{-1}), while a subtropical thunderstorm also analyzed during the campaign had a production rate of ~140-210 moles flash^{-1} (Huntrieser et al., 2008).

Huntrieser et al. (2009) analyzed thunderstorms sampled over Northern Australia during the SCOUT-O3/ACTIVE field experiment with results similar to the Brazilian thunderstorms. On 19 November 2005, tropical continental thunderstorms generated lower LNO_x production rates (121 moles flash^{-1}) compared with subtropical continental (385 moles flash^{-1}) and Hector (292-343 moles flash^{-1}) thunderstorms. Like the thunderstorms observed during TROCCINOX, the estimated vertical wind shear over Northern Australia between the anvil outflow and steering level was greater in subtropical (~15 m s^{-1}) versus tropical (~6 m s^{-1}) convection. For Hector thunderstorms a different process may be responsible, where the presence of multiple storm centers from merging convective cells may lead to longer flash lengths. The premonsoon season flight discussed by Huntrieser et al. (2009), measured enhanced upper tropospheric NO_x only within storm systems (Labrador et al., 2009), while later in the ACTIVE experiment (e.g., January 2006) enhancements in LNO_x were found over widespread regions.

Mesoscale convective systems (MCSs) over West Africa were analyzed during the African Monsoon Multidisciplinary Analysis (AMMA) wet season field campaign (Huntrieser et al., 2011). Unlike the Brazilian (Huntrieser et al., 2008) and Australian (Huntrieser et al., 2009) thunderstorms, the AMMA MCSs showed a greater influence from boundary layer versus lightning NO_x. The tropical and subtropical MCSs investigated during AMMA indicated LNO_x production rates (70 moles flash^{-1} and 179 moles flash^{-1}, respectively) were comparable to those observed in similar air mass thunderstorms during TROCCINOX. Unlike the tropical and subtropical thunderstorms observed during TROCCINOX and SCOUT-O3/ACTIVE, the difference in vertical wind shear (defined as the difference between the anvil outflow and

steering level wind vectors) between subtropical and tropical AMMA MCSs was not as large (7 m s^{-1} and 9 m s^{-1}, respectively).

Based on the results from the tropical field campaigns, thunderstorms closer to the equator generally have lower LNO_x production rates, and convection over Northern Australia tend to exhibit higher production rates than storms observed in Brazil and West Africa (Höller et al., 2009). Although previous research has characterized thunderstorms based on the type of air mass in which the cell developed (e.g., tropical air mass) and not by the geographic location, it is important to note that storms that evolve over the same area (e.g., tropical northern Australia) cannot be placed into one specific category of convection, as thunderstorms may develop within different climate regimes over the same location. May and Ballinger (2007) point out the differences in convection near Darwin, Australia, during the buildup/break and monsoonal regimes. Storms that occur in the buildup/break regime are representative of continental tropical convection and are generally tall, small in size, long-lived, and intense. The opposite is true of thunderstorms during the monsoon season, which are considered more maritime tropical, even though they occur over the same geographic area. Therefore, an investigation of a greater variety of storm types and environmental conditions would provide additional estimates of LNO_x production rates and help reduce the large uncertainty that still exists for estimating and modeling the global LNO_x production rate. Labrador et al. (2005) highlight this need while investigating a "best" source magnitude and vertical placement of LNO_x. It is indicated the uncertainty also lies in a lack of understanding the amount of energy, and associated NO molecules, produced per lightning discharge, as well as the horizontal distribution of lightning.

The in-situ measurements made during SCOUT-O3/ACTIVE over the "Maritime Continent" (the Indonesian archipelago, north Australia, and New Guinea) are well-suited for

studying LNO_x with a cloud-resolving model. Previous modeling studies indicate the feasibility of incorporating observations into numerical thunderstorm simulations in this region. This leads to consideration of how NO production per flash in a Hector storm compares with those at higher latitudes and with other storm types in the tropics. This paper contains the first cloud-resolved LNO_x simulation performed in the deep tropics for a storm with detailed lightning and anvil NO_x observations.

2.3 Numerical Simulations of Hector Thunderstorms

The "Maritime Continent" is one of the primary regions of global latent heat release that contributes to the forcing of the planetary-scale Hadley and Walker circulations. Global climate variations are directly influenced by changes in latent heat release and radiative heating within this region. During the transition season (November-December), characteristic diurnal convection is detected on 65-90% of days over a pair of relatively flat islands, called the Tiwis, north of Darwin, Australia (Saito et al., 2001). Together the Tiwi Islands (Fig. 1) are about 150 km west-to-east and 50 km north-to-south (Crook, 2001). The islands are excellent laboratories for studying geographically fixed tropical convection due to their diurnal cycle of latent heat release. The storms, locally known as Hector, can reach heights of 20 km, allowing them to be viewed from locations, like Darwin, that are 100 km away (Crook, 2001).

The Island Thunderstorm Experiment (ITEX) occurred over the Tiwi Islands in 1988 to facilitate improved understanding of tropical island convection. Golding (1993) numerically simulated Hector using the U.K. Met Office mesoscale model and information from ITEX. While simulations showed some agreement with observations, the model placed convergence near the island's center when it was actually located near the south coast. Simulations

demonstrated an island-scale confluence of sea breezes, cold pool interactions among breeze-forced storms, and storm development with little sensitivity to changes in cloud microphysics.

To further study deep island-based convection, the Maritime Continent Thunderstorm Experiment (MCTEX) was conducted in November-December 1995. Using observations from MCTEX, Carbone et al. (2000) created a conceptual model of Hector development. Carbone et al. (2000) suggest a flat, elliptical island of order 100-km resolution can act as an heat source and create an optimal condition for the initiation, organization, and propagation of convection. The MCTEX simulations by Saito et al. (2001) found that the diurnal evolution of convective activity over the Tiwi Islands consisted of five stages, which capture the transition from horizontally to vertically forced convection. Shallow, non-precipitating convective cells develop over the island interior, as well as within and ahead of the sea breeze fronts during the dry and condensation stages in the morning. By afternoon the convection is forced into the vertical as sea breeze fronts from opposite sides of the island move farther inland (precipitating stage), interacting near the leeward coast and causing a sudden increase in convective activity (merging stage).

The majority of Hector thunderstorms develop upon the interaction of the sea breeze and gust fronts from earlier convection. Simulations suggest the convective strength of a system increases as wind speed decreases and as wind direction turns toward the major axis of the island (Crook, 2001). If convection can free itself from the sea breeze maintenance mechanism, it can feed on the heated island boundary layer when evaporatively produced cold pools become cooler than the nearby sea breeze. Thus, the convective strength, which was found to increase with increasing heat and moisture fluxes, was more sensitive to heat flux (Crook, 2001). But as daytime heating decreases, so does the convective activity (decay stage). The diurnal evolution indicated the horizontal island circulations, created in large part by the size and shape of the

islands, and the vertical stability of the atmosphere both play important roles in the strength of the island convection.

Since deep island convection, like Hector, can penetrate the tropopause, numerical simulations are used to investigate the influence Hector thunderstorms have on the moisture in the upper troposphere and lower stratosphere. In the deep convective updrafts of overshooting tops, ice particles form in the rapidly cooling air and, if large enough, settle out and dehydrate the lower stratosphere (Chemel et al., 2009). If ice particles are not removed via sedimentation, their presence increases the potential for air to moisten by evaporation as particles slowly descend. Chemel et al. (2009) simulated the 30 November 2005 Hector storm observed during the SCOUT-O3/ACTIVE field campaign. The simulation indicated occasional overshooting tops affect the moistening or dehydration of the lower stratosphere via convective ice lofting. However, the impact of episodic vertical transport of short-lived boundary layer chemical species on the lower stratosphere was not investigated (Chemel et al., 2009).

3 Observations

This study focuses on a single-cell Hector storm observed on 16 November 2005 during the SCOUT-O3/ACTIVE (Brunner et al., 2009; Vaughan et al., 2008) field campaigns based in Darwin, Australia. Figure 2 shows a series of two photographs documenting the development of the Hector thunderstorm over the Tiwi Islands. This storm and its vicinity were sampled by the DLR Falcon, M55 Geophysica, Australia's Grob G520T Egrett, and the U.K. Natural Environment Research Council Dornier aircraft. Two radars owned and operated by the Centre for Australian Weather and Climate Research (CAWCR) were used on this day: the Darwin Berrimah Doppler radar and the C-Band Polarimetric (CPOL) radar based near Gunn Point. A

lightning detection network (LINET) (Betz et al., 2004, 2007, 2008; Höller et al., 2009) of six stations was also established: Point Stuart, Cape Don, Pirlangimpi, Darwin, Dundee Beach, and Mount Bundy. Figure 1 provides the location of the radar and LINET stations. LINET detects individual strokes, which were then organized into flashes based on time of occurrence (within 1 s) and location (within 10 km). Flash data were obtained from 13:30 LT to 19:30 LT for the Hector storm of interest, although LINET collected data over the region for the entire day. Darwin rawinsondes were also available on this day.

Hector first appeared on radar at 14:28 LT over Apsley Strait between Melville and Bathurst Islands. Radar imagery shows the cell generally moves westward as it intensifies by 14:58 LT, reaching a peak radar reflectivity of roughly 60 dBZ by 16:00 LT. Satellite imagery indicates anvil development by 15:03 LT. By 16:38 LT, radar observations indicate the storm had begun to weaken and the anvil moved toward the south in response to the northerly upper tropospheric winds. Over the cell lifetime the anvil had an average area of 2365 km^2 based on IR satellite images and the Droplet Measurement Technology (DMT) cloud, aerosol and precipitation spectrometer (CAPS) on board the Egrett. The cell is nearly dissipated by 18:28 LT based on radar.

The Geophysica approached the developing single-cell from the north, descending stepwise from 19 km to the anvil top, arriving as the detached anvil was already moving south. As the main convective activity was advected west, the Geophysica headed back northwest to sample overshoots of the cell, but ultimately returned to probing the environment above the main anvil by slowly descending into the cloud top. The two anvil transects made by the Geophysica occurred from roughly 11-17 km over the period 17:44-18:21 LT. The Falcon initially flew further north, sampling outflow from a large mesoscale system that had previously developed

over Papua New Guinea. The Falcon returned to the area south of the Tiwi Islands where it flew east-west cross-sections below the anvil, characterizing its vertical structure by lidar. The Egrett aircraft, which most extensively sampled anvil cloud air above the Falcon from roughly 13.2-13.8 km, began its first northeast-southwest oriented transect at 16:57 LT and completed its final anvil pass at 18:49 LT. The Dornier characterized low-level inflow by flying large circles around the active cells. A cross calibration was performed on site in Darwin to ensure that differences in calibration standards did not cause variation in measurements amongst the aircraft.

4 Numerical Model

The WRF version 2.2 model used a simple gas and aqueous chemistry scheme (WRF-AqChem) to simulate the Hector thunderstorm. WRF-AqChem is described in detail by Barth et al. (2007a) and the WRF meteorological model is described by Skamarock et al. (2005). This model uses nonhydrostatic compressible equations. The ice microphysics scheme (Lin et al., 1983) predicts the mass mixing ratios of cloud water, rain, cloud ice, snow, and hail. The model contains basic O_3-NO_x-CO chemistry online with 16 chemical species in the gas phase and the five hydrometeor reservoirs. Diurnally-varying clear-sky photolysis rates as a function of altitude are derived from the Troposphere Ultraviolet and Visible (TUV) radiation code (Madronich and Flocke, 1999). Overhead cloudiness is not accounted for in the TUV code. Therefore, the photolysis rates may be underestimated in the upper portion of the cloud and overestimated below, affecting the partitioning of NO and NO_2. However, this is not a concern because we evaluate the model NO_x (sum of NO and NO_2) against NO_x observations. Other effects on chemistry (e.g., loss of NO_2 to HNO_3; O_3 production) will be minor over the short duration of the storm. Aqueous chemistry is computed for cloud water and rain. Partitioning of

species between gas and liquid hydrometeors is assumed to be in Henry's Law equilibrium for most species, but diffusion-limited mass transfer partitions highly soluble or highly reactive species. Transfer of species also occurs during the transformation of gas to ice and between hydrometeor categories following the microphysics processes. LNO_x production is implemented using the DeCaria et al. (2000, 2005) schemes.

For this simulation, the model is configured to a 300×150×25 km domain with 300 grid points in the east-west direction and 150 grid points in the north-south direction at 1 km resolution and 60 grid points in the vertical direction with a variable resolution beginning at 40 m at the surface and stretching to 1840 m at the top of the domain, which is 25 km. The Tiwi Islands are represented by a landmask in the model with sensible heating at the surface applied following sunrise at 40% of solar flux (Crook, 2001). Lightning channel segments do not follow a uniform vertical distribution (MacGorman and Rust, 1998). Instead, the vertical distribution of CG and IC flashes follow single and bimodal Gaussian distributions, respectively, where the peaks indicate the maximum negative charge in the cloud (DeCaria et al., 2000). For this simulation, the lightning channels are set to maximize at -15ºC and -60ºC, or ~7.0 km and ~12.7 km, respectively. The channels are similar to midlatitude thunderstorms (-15ºC and -45ºC), except with a colder upper mode isotherm assumption due to the greater tropopause height in the tropics. The mean altitude of IC flashes for all types of observed storms over the 2005-2006 season was 12.2 km based on LINET observations. However, we would expect this altitude would be greater than 12.2 km in Hector storms, but we cannot be certain of the actual altitude for this particular storm. A more in depth analysis of the LINET data with regard to the vertical placement of IC flashes during our Hector storm is beyond the scope of this paper. NO production is tested at both 450 and 500 moles per CG and IC flash, which are approximately the

mean values from the series of midlatitude and subtropical event simulations (Ott et al., 2010) described in Section 2.1. These values are used to determine whether NO production per flash in the Hector storm is similar to that in midlatitude or subtropical storms.

The model was initialized with a horizontally-homogeneous environment using an atmospheric profile constructed from an early morning (08:30 LT) Darwin sounding (Fig. 3) and surface observations. Modifications were made to the temperature and moisture profiles using observations from a low-level Dornier flight and the boundary layer winds were adjusted to allow convection to form over the desired location. The sounding had a convective available potential energy (CAPE) value of 1360 J kg^{-1}. The initial chemical profiles for CO, O_3, NO, and NO_2 were constructed from a composite of Dornier, Falcon, Geophysica, and Egrett aircraft data (Fig. 4). These data were restricted to times when the aircraft were located out-of-cloud and positioned primarily to the north of the developing cell. The vertical intervals of data used in the profile construction depended on the availability of data from each aircraft. For CO and O_3, a combination of Dornier and Geophysica values were used from the surface to 3.5 km. Between 3.5-5 km, vertical layers were interpolated from the values at 3.5 km and 5 km. Above 5 km, Geophysica observations were used, except between 10-14 km where Egrett and Geophysica CO observations were averaged and smoothed. The CO profile shows spikes up to 125 ppbv in the lowest 3 km of the boundary layer, which is most likely due to upwind biomass fires in northern Australia (Allen et al., 2008). When biomass burning did not occur under premonsoon conditions in the same field campaign, the average CO values for the lowest 3 km were roughly 85 ppbv (Allen et al., 2008). For NO and NO_2 values, Falcon averages were used below 9 km and Egrett averages were used above this altitude. The NO and NO_2 profiles are enhanced in the upper troposphere due to upwind lightning.

The meteorological simulation was initiated at sunrise (07:15 LT). Chemistry and trace gas transport were started in the model at 4 hours 30 minutes into the simulation (11:45 LT), which is just prior to the initial development of the main Hector cell of interest in the model. Convection intensified in the model simulation about 2 hours earlier than in the observations (see Sect. 5). Therefore, the observed LINET flashes from the storm of interest, which occurred in real time between 14:48-17:48 LT (Fig. 5), were read into the model at 10-second intervals beginning at 5 hours 20 minutes into the simulation (12:35 LT). Figure 6 illustrates the progression of LINET strokes from east-to-west with time. To keep the lightning flashes within the cell of interest, lightning flash rates read into the model were restricted using a spatial mask that was adjusted at 10-minute intervals based on the movement of the cell within the model domain. There were 438 CG flashes with a mean absolute peak current value of 17.3 kA and 683 IC flashes with a mean absolute peak current value of 9.6 kA. The absolute values do not distinguish between negative and positive stroke signs. Observed flash rates peaked at approximately 15:40 LT (~30 total flashes min^{-1}), with a secondary peak at roughly 16:20 LT (~10 total flashes min^{-1}), which was followed by an extensive period of low flash rates (Fig. 5).

Flash rates were also estimated using model simulated storm parameters and six different FRPSs used by Barthe et al. (2010). Table 2 lists the six FRPS equations. The WRF-AqChem 10-minute interval output was used in flash rate calculations offline to compare the trend and number of total flashes over the lifetime of the observed and simulated 16 November 2005 Hector thunderstorm. A scaling factor was applied to each FRPS and the offline calculations were rerun in order to select the FRPS(s) whose modeled flash rate trends best matched the observations. The adjusted equations for the selected FRPSs were then incorporated into the WRF-AqChem model, so the model simulated flashes could be substituted for the observed

LINET flashes and the resulting LNO_x associated with each of the selected FRPS(s) compared against the simulated LNO_x produced by the observed flashes.

5 Results and Discussion

5.1 Meteorology

The WRF-AqChem idealized simulation reproduced a number of features of the observed storm (Table 3). Given the simulation begins at sunrise (07:15 LT), the simulated single-cell is assumed to begin at 11:55 LT, roughly 2.5 hours earlier than the observed cell. The Geostationary Meteorological Satellite 5 (GMS-5) first saw the anvil at 15:03 LT, while the model indicates a two hour offset with initial anvil formation at 13 km occurring at 12:55 LT (5 hours 40 minutes simulation time). The modeled cell achieves its peak radar reflectivity of ~65 dBZ at 14:15 LT. This is close to the observed peak radar reflectivity of ~60 dBZ at 16:00 LT, with a time offset of 1.75 hours. By 15:35 LT in the model, the anvil detached from the storm core and is blown toward the south.

The modeled anvil at 13 km dissipates by 16:15 LT (9 hours simulation time) though satellite observations indicate the anvil dissipated by 18:03 LT. Thus, the anvil dissipation offset is 1.75 hours. The simulated cell dissipates in the model computed radar reflectivity at 2.5 km altitude by 15:55 LT whereas radar observations show the cell dissipating by 18:28 LT, indicating an offset of 2.5 hours. These time offsets between model and observations indicate that the simulation was on average 2 hours earlier than observations. It may be when the low-level winds were modified to initiate convection in the correct location, that an earlier convergence of winds occurred. It is also possible that initializing the model with a sensible heat

source of 40% of solar flux was too large and accelerated the onset of the storm, but as indicated above, the general features of Hector were still captured by the simulation.

The model computed radar reflectivity at 2.5 km altitude (Fig. 7 bottom) is compared with the observed radar from Gunn Point (Fig. 7 top) at an equivalent time in the storm life cycle. Both the model and the observations show the Hector cell over Bathurst Island and other scattered cells to the east. Vertical cross sections of model-computed radar reflectivity along an angle 130º from the north through the core of the storm can be compared with observed vertical radar cross sections from Gunn Point (Fig. 8). Note that Figure 8 shows vertical cross sections through the observed cell (top panel) and developing model storm (bottom panel) from the southeast to northwest (left to right). In the observations, the 20 dBZ contour (cyan) extends to 16 km. In the model simulation, the 20 dBZ contour extends to roughly 16.5 km. However, the observed 50 dBZ contour (red/magenta interface) is roughly 7 km wide and reaches 4 km in altitude, while the model simulation indicates the 50 dBZ contour extends to an altitude of 12.5 km and ranges in width from ~10 km near the surface to ~18 km around 5 km altitude. The simulated anvil slopes downward in Figure 8 (bottom panel) away from the storm core, unlike the structure of the observed anvil. Differences in the observed and simulated 50 dBZ contour and anvil structure in the radar reflectivity may be due to how the ice mass concentrations are calculated in the WRF-AqChem model, which uses a bulk microphysics scheme. Overestimates of reflectivity values in the middle to upper troposphere are a well-known bias common to many bulk microphysical schemes in simulations of tropical convective systems (Lang et al., 2011). Dahl et al. (2011a, b) indicate that environments where gust fronts and sea breezes collide, as over the Tiwi Islands, and high shear environments, as in the midlatitudes, can lead to an enhancement in graupel area within a simulated storm. The simulated total hydrometeors

indicate the model cloud overshoots to 20 km, which is typical of a Hector storm. The anvil hydrometeors may slope down and away from the simulated storm core due to a downward vertical motion at the storm's edge in response to the slight overestimation in upward transport within the core (see Sect. 5.2). It is also possible the sedimentation was too strong in the model, causing the downward slope. Chemel et al. (2009) showed the anvil in their simulated 30 November 2005 Hector storm also appeared to slope away from the core. The horizontal extent of the storm core and precipitation region in our Hector storm is about the same for both model results and observations (~40 km), as is the extent of the anvil beyond the precipitation region.

Comparison of the anvil size from IR satellite images and Egrett in-cloud flight passes to modeled total hydrometeors at 13 km indicates anvil size in the simulation is comparable to both types of observations (Fig. 9). The average anvil extent over the cell lifetime is obtained from satellite observations and the DMT CAPS onboard the Egrett aircraft between 15:03-18:03 LT and 17:01-18:30 LT, respectively, and is estimated to be roughly 2400 km^2. This estimate is slightly smaller than the model estimate of the average anvil extent at 13 km (2757 km^2) during the simulated anvil's lifetime (12:55-16:15 LT). Overall, the simulated storm structure compares favorably with observations, except for the extent of the 50 dBZ contour.

5.2 Carbon Monoxide

Figure 10 shows a time series of vertical cross sections of CO mixing ratios from 12:55 LT (5 hours 40 minutes simulation time) to 15:25 LT (8 hours 10 minutes simulation time) through the simulated cell. Air that initially contained the maximum CO mixing ratios exceeding 100 ppbv in the 0-4 km region is transported to over 16 km in the core updraft region and over 14 km in the anvil, indicating strong upward motion. In fact, modeled vertical velocities reached a maximum of 30 m s^{-1} in the core of the storm. Both the core and downwind anvil regions of the

storm are largely composed of air that resided in the boundary layer prior to convection, while entrainment of environmental air with lower CO mixing ratios appears to be minimal.

Mixing ratios observed by the Egrett aircraft during the series of five anvil penetrations over the period 16:57-18:49 LT were compared with the simulated tracer transport from 12:55-14:45 LT where anvil-in-cloud conditions were present (total hydrometeors ≥ 0.01 g kg^{-1}). Data collected by the Egrett were averaged over 11-s intervals to yield a spatial scale equivalent to the model grid cell size. The mixing ratio statistics and specified initial conditions are shown in Tables 3 and 4 for lightning NO production scenarios of 450 and 500 moles flash^{-1}. Given that differences in the simulated CO mixing ratio statistics between the two scenarios are small, we will focus on the results from the lightning NO production scenario of 500 moles flash^{-1}, which are closer to the observations. The simulated CO mixing ratio statistics within the 0.71 km thick model layer centered at 13.4 km best match those based on the available Egrett observations between 13.2-13.8 km (Table 4), indicating vertical transport is generally well simulated by the model. Figure 11 shows the calculated probability density functions (PDFs) of observed and simulated CO. The simulated convective transport increases CO values above the initial condition (70.1 ppbv) at many grid points, but the simulated and observed PDFs have significant differences. Egrett observations indicate a strong peak between 80-85 ppbv with just over 25% of CO observations and a secondary peak between 95-100 ppbv with 12% of the observations. The model distribution also shows two peaks, but they are slightly offset from the observations. Roughly 18% of the simulated CO mixing ratio values are within the primary peak between 70-75 ppbv and a broader secondary peak covers the bins from 100-110 ppbv with roughly 9-10% of the simulated mixing ratios in each bin. The model simulation produces CO mixing ratios less than 65 ppbv at this altitude, which are not observed, and most likely the result of downward

transport from higher altitudes in the model. In general, the model produces more extreme values, both large and small, than the observations. However, the total percentage of model anvil values greater than 80 ppbv was 57%, closely matching the 62% found in the observations in the same layer. The simulated convection increases the mean value at 13.4 km to 85.8 ppbv from the initial condition of 70.1 ppbv given 500 moles NO flash^{-1}, slightly exceeding the observed value of 84.0 ppbv by 1.8 ppbv of simulated CO.

The raw tracer mixing ratios measured by the Geophysica were averaged over 5-s intervals between 17:44-18:21 LT and compared against the simulated tracer transport from 12:55-14:45 LT (Table 6). In the layers centered at 11.4-14.1 km the simulated CO mixing ratios overestimate the Geophysica observations by roughly 25-35% and reasonably replicate the values within ±10% from 14.9-16.6 km. The overestimation is partially due to the CO profile used to initialize the model, which was constructed using averages of the Egrett and Geophysica observations for each model layer between 10-14 km. The resulting mixing ratios in this portion of the profile (70-75 ppbv) are slightly higher than those observed by the Geophysica in cloud-free air (65 ppbv). Correcting for this 10-15 ppbv offset would reduce the model overestimates to 0-20%. Cloud observations from the Geophysica indicate the aircraft passed in and out of the anvil (e.g., flew near cloud edge) and therefore, these data may not be representative of the anvil in general. The Geophysica CO observations show only minor effects (1-4 ppbv) of convective transport, but these data represent only a very small sample of the cloud air compared with that of the Egrett (see number of observations in Tables 4 and 6).

5.3 Nitrogen Oxides

5.3.1 NO_x Mixing Ratios

The CO analysis indicated small errors in simulated vertical transport, so it may not be necessarily correct to only compare observed and modeled trace gases from the same altitudes. In addition, there is uncertainty concerning the altitude where lightning channels maximize in the upper part of the cloud. Therefore, the NO_x mixing ratio comparison with observations focuses on the model layers centered at 12.0 km, 12.7 km, and 13.4 km.

For a simulation without lightning NO production, convection brings lower NO_x mixing ratios upward to anvil levels (Fig. 12). At 14:45 LT in the simulation, at the end of the aircraft sampling period, the average NO_x mixing ratio within the layers centered at 12.0 km and 12.7 km are 60 pptv and 75 pptv, respectively, compared to 140 pptv in the layer centered at 13.4 km at the start of the simulation. These are 57% and 46% decreases, respectively, largely due to convective transport.

The simulation with lightning tested two lightning NO production scenarios. The 500 mole $flash^{-1}$ scenario is based on the results of Ott et al. (2010) for midlatitude and subtropical thunderstorms, while the 450 mole $flash^{-1}$ scenario represents a 10% perturbation. Egrett NO_x observations are based on sequential NO and NO_x sampling. For the times when just NO was measured, a photostationary state calculation was used to estimate NO_x using observed NO values, model O_3 mixing ratios, temperature from the Darwin sounding, and $J(NO_2)$ from the TUV model. Table 5 indicates the model underestimated the mean anvil NO_x when 450 moles NO is used, while 500 moles NO provides a closer estimate of the Egrett observations in the mean, especially for the model layer centered at 12.0 km. These results show that mean NO_x mixing ratios in the anvil are approximately linearly related to the LNO_x production rate per

flash (~10% reduction in mixing ratios for 10% reduction in LNO_x production per flash). Given these results, the remainder of the NO_x analysis focuses on the lightning NO production scenario which uses 500 moles NO $flash^{-1}$. However, the mean anvil mixing ratio at 13.4 km is 705 pptv, which is less than the observed value (Table 6). Therefore, using the demonstrated linearity we cannot rule out a mean LNOx production of 600 moles $flash^{-1}$. For a simulation with lightning NO production (using the DeCaria et al. (2005) scheme with parameters as specified in Sect. 4), NO_x mixing ratios exceed 3 ppbv in the storm core (Fig. 13). Downwind of the storm core, anvil NO_x values slightly exceed 3 ppbv for roughly a 25 km distance (Fig. 14). The finding of NO_x production of 500 moles $flash^{-1}$ or larger is consistent with that estimated for CG flashes (523 moles $flash^{-1}$) based on the observed mean peak current using the relationship given by Price et al. (1997). If the Price et al. (1997) relationship is assumed to also hold for IC flashes, one would obtain an estimate of 291 moles $flash^{-1}$. The model results clearly indicate an NO production per IC flash larger than this value is needed to match observed anvil NO_x observations.

The PDFs in Figure 15 compare the distribution of model NO_x centered at 12.0 km and 12.7 km with the Egrett observed NO_x. For either layer, the model NO_x PDF did not match the shape of the observations well. Though the mean anvil-level NO_x in both model layers adequately reflects the mean of the Egrett anvil-level observations, a substantial fraction of observations between 200-400 pptv and above 2400 pptv are missing from the simulated NO_x. The Egrett observations >2400 pptv may be from relatively fresh lightning flashes encountered by the aircraft and not captured with the DeCaria et al. (2005) scheme, which places NO_x into the model cloud in bulk fashion. In this scheme the NO production is injected within the 20 dBZ contour of the storm and according to prescribed Gaussian vertical distributions (e.g., not along

specific channels). As a result, the model standard deviation remains smaller than observed by 43% and the upper end of the distribution is slightly underestimated. A broad secondary peak in model-simulated NO_x occurs in the bins between 1000-2400 pptv, overestimating the Egrett observations. Therefore, the magnitude of the NO_x peaks seen in the aircraft data are not reflected in the model results, which indicates that individual model grid cells contain smaller NO_x peaks than the observations. Future improvements to this simulation should include a LNO_x parameterization (Ott et al., 2007; Barthe and Barth, 2008) that would inject NO_x along specific channels of individual flashes.

The simulated NO_x mixing ratios underestimate the Geophysica measurements within the layers centered at 13.4-14.9 km, and overestimate the observations at the other layers (Table 6). The underestimation by the model may be due to the Geophysica sampling a number of fresh lightning flashes whereas the model values are more representative of lightning emissions that are more dispersed, as indicated by the smaller standard deviations in the simulation. Strong vertical motions within the simulated storm likely bring enhanced NO_x mixing ratios from injected lightning at mid-cloud and from the stratosphere, leading to an overestimation of observed NO_x. Uncertainty in initial conditions may also cause an overestimation in NO_x, as the Geophysica measured smaller values just inside the edge of the anvil during the storm in the lower and upper layers compared with the mean Egrett out-of-cloud values used in the initial conditions profile.

5.3.2 NO_2 Column Amounts

LNO_2 satellite observations have been described by Boersma et al. (2005), Beirle et al. (2009, 2010), and Bucsela et al. (2010). The importance of investigating LNO_2 signals with satellite observations is to identify regional differences in thunderstorm contribution to NO_2 (Beirle et al.,

2010). Here the NO_2 column analysis provides the NO_2 satellite retrieval community with potential outflow expectations for a highly electrified, high NO_x producing storm. Figure 16 shows the maximum simulated NO_2 tropospheric column values that potentially could be observed for the Hector storm by satellite from the tropopause to 400 mb and 600 mb at 14:45 LT. These are pressures within a thunderstorm cloud to which NO_2 is thought to be observable from space. Actual visibility of LNO_2 from satellite may differ from these values due to the particular radiative transfer characteristics of the cloud. The largest mean partial NO_2 column values ($\geq 60\times10^{14}$ molecules cm^{-2}) are located along and just south of Apsley Strait. Low-level radar reflectivity indicate Hector is on the western coast of Bathurst Island prior to 14:45 LT (Fig. 7). With northerly upper level winds (Fig. 3) and a westward motion of the storm track across the Tiwi Islands, NO_2 is transported away from the storm core and along the anvil, explaining the placement of the large mean NO_2 column values. However, the Ozone Monitoring Instrument (OMI) on NASA's Aura satellite passed over at ~13:30 LT, which was too early to observe the LNO_x from Hector. A LNO_2 signal was not found during the OMI over pass at ~13:30 LT or ~15:00 LT. There is still much uncertainty in observing LNO_2 from space, as the NO_2 signal is detected by satellite for some thunderstorms and not others (Beirle et al., 2010).

Tropospheric column NO_2 from the simulated Hector storm is compared with columns computed from midlatitude storm simulations (Ott et al., 2010) and with OMI observations for tropical marine thunderstorm events from NASA's Tropical Composition, Cloud and Climate Coupling (TC^4) experiment near Costa Rica and Panama (Bucsela et al., 2010). Ott et al. (2010) indicated partial NO_2 column amounts peaked over similar regions (relative to the storm core) in the simulated storm anvils during CRYSTAL-FACE (Cirrus Regional Study of Tropical Anvils

and Cirrus Layers – Florida Area Cirrus Experiment), STERAO, and EULINOX. In the Hector storm cloud the mean partial NO_2 column amounts from 400 mb to the tropopause (Fig. 16 left panel) are the same order of magnitude as the storms from CRYSTAL-FACE, STERAO, and EULINOX. The maximum partial NO_2 column amounts from the tropopause to 400 mb (~84×10^{14} molecules cm^{-2}) and 600 mb (~103×10^{14} molecules cm^{-2}), following the end of lightning flash injections into the model, indicate the in-cloud column amounts fall within the range of peak values for the subtropical and midlatitude storms analyzed by Ott et al. (2010), but are larger than those found in the TC[4] storms (~45×10^{14} molecules cm^{-2}).

5.3.3 NO_x Vertical Profiles

Vertical profiles of the average in-cloud simulated NO_x mixing ratios with and without lightning were compared at 13:55 LT (Fig. 17). In the lightning simulation two large NO_x peaks (~0.95-1.05 ppbv) occur around 8.5 km and 13.5 km. The peak at 13.5 km is ~0.8 km higher than the prescribed upper mode (-60º isotherm) height in the LNO_x vertical distribution, while the peak at 8.5 km is roughly 1.5 km higher than the prescribed lower mode (-15º isotherm). Secondary peaks are also noted near the surface and around 6 km with ~0.5 ppbv and ~0.75 ppbv NO_x, respectively. Without lightning, the profile is similar to the initial NO_x chemical profile in Fig. 4 in the lower troposphere, but upward transport caused upper tropospheric values to be lower than the initial conditions. With lightning, the peaks in NO_x mixing ratios are likely due to a combination of the lightning injection location and vertical transport within the cloud.

The cloud-resolved model analysis of Pickering et al. (1998) produced average profiles of LNO_x mass for midlatitude continental, tropical continental, and tropical marine regimes all showing peaks in mass near the surface and in the upper troposphere. These C-shaped vertical distributions of LNO_x mass were adopted by many global chemical transport models (CTMs).

Ott et al. (2010) produced an updated set of LNO_x mass profiles for midlatitude and subtropical storms using a more realistic scheme of vertical placement of LNO_x in the cloud-resolved model. For additional comparison against tropical convection, Figure 18 shows the percentage of N mass per kilometer due to LNO_x for this idealized Hector simulation following the end of model convection at 15:35 LT. Approximately 85% of the simulated LNO_x is located above 7 km. The maximum peak in total lightning N mass (~20%) is located within the layer centered at ~7.5 km and roughly corresponds to the lower mode of the vertical distribution of the LNO_x source. A second peak (~9.5%) around ~13.5 km is ~0.8 km higher than the upper isotherm (-60ºC). The vertical distribution did not resemble the tropical continental profile hypothesized by Ott et al. (2010), which had a dominant peak at 11-14 km. Instead, the vertical profile of the percentage of LNO_x mass per kilometer for our Hector storm resembles the average midlatitude continental profile from Ott et al. (2010), except shifted ~3 km higher in altitude. It is possible the directional shear within this storm, discussed below, played a key role in the profile shape.

Based on these results, a lightning NO production scenario of 500 moles $flash^{-1}$ in this Hector storm is roughly equivalent to the mean of the midlatitude and subtropical events previously studied with a similar approach. The wind speed difference, on the other hand, in the 850-200 hPa layer is only 5 m s^{-1} in the Hector system compared to the 20 m s^{-1} and 30 m s^{-1} variation in wind speed between similar pressure levels for the STERAO and EULINOX midlatitude cases. Wind direction variation in the Hector storm, however, is significant, with wind direction turning from southeast to northwest with increasing height between the low- and upper-levels of the atmosphere, respectively (Fig. 3). This led to horizontal stretching of the storm system and possibly longer flash lengths than may be typical in the tropics. Hector, and other tropical island convection driven by localized surface heating, may create more powerful

storms that are not representative of other types of tropical thunderstorms. This Hector storm, along with another Hector system documented by Huntrieser et al. (2009), indicate NO production per flash is larger than most other tropical thunderstorm events in the literature.

5.4 Ozone

Model O_3 between 12:55-14:45 LT ranges from 6.6-18.6 ppbv in the anvil model layer (centered at 13.4 km) sampled by the Egrett due to both upward and downward transport, compared with the initial condition of 10 ppbv. Vertical cross sections of O_3 mixing ratios for simulations without and with lightning (Fig. 19) show the upward and downward movement of O_3 within the storm at 13:35 LT, a time of peak anvil NO_x production within the model layers centered between 12.0-13.4 km. The vertical cross section with lightning shows O_3 mixing ratios are ~4 ppbv lower between 6-15 km in the storm core when compared with the vertical cross section without lightning. Substantially larger NO_x mixing ratios are produced by simulations run with versus without lightning (Figs. 12-13), suggesting LNO_x had a role in O_3 titration in the cloud. This effect had also been noted in previous research (Wang and Prinn, 2000; Ott et al., 2007). A comparison to observations cannot be performed at the 12.0 km and 12.7 km altitudes, as the Egrett did not measure O_3 on this flight. The upward transport of low O_3 from the lower troposphere and titration of O_3 by LNO_x decreases the O_3 baseline in the upper troposphere prior to the initiation of downwind O_3 production. It is desired to determine how much O_3 is produced downwind of a thunderstorm following convection, however, our Hector simulation did not run past the end of the storm. Therefore, we can only provide the start of an answer concerning the overall impact of this storm on O_3, especially when O_3 production most likely started after the end of the simulation.

5.5 Flash Rate Parameterization Schemes

The lightning observed during the Hector thunderstorm occurred between 14:48-17:48 LT with two peaks in flash rates and 1094 total lightning flashes. The observed three hour flash rate trend is overlaid onto the flash rates predicted from six different model parameters (Fig. 20). The predicted flash rates are assumed to begin at the same time the observed flash rates were begun in the model (12:35 LT). Figure 20 compares the observed and modeled instantaneous lightning flash rates (flashes per minute) at 10-minute intervals over the lifetime of the Hector thunderstorm. Most of the scaling factors needed to be applied to the FRPS equations to reduce the total flashes to approximately match the observed total flashes were larger than 1/10. While the ice mass flux product scheme required the smallest scaling factor (~1/57), a scaling factor of roughly 1/3, 1/8, and 1/10 were needed for the cloud top height and updraft volume, maximum vertical velocity and ice water path, and precipitation ice mass FRPS equations, respectively. However, the maximum vertical velocity and cloud top height FRPSs produce a lightning flash rate trend that best matches the primary and secondary peaks in the observed flash rates. The lightning flash rates per minute for the selected FRPSs and the LINET observations are shown in Figure 21. The total numbers of simulated flashes calculated between 12:35-15:35 LT for the maximum vertical velocity and cloud top height FRPSs are ~ 994 and ~1124, respectively, which are both within 10% of the observations. The maximum vertical velocity and cloud top height FRPSs both indicate primary peaks that are larger and slightly smaller in magnitude, respectively, and occur earlier (~13:00 LT) than the observed primary peak (~13:40 LT). Figure 21 also shows that around the time of the observed secondary peak the maximum vertical velocity and cloud top height schemes have two peaks of slightly greater and similar magnitude, respectively.

Vertical cross-sections of model NO_x at 13:25 LT indicate that the maximum vertical velocity and cloud top height parameters in the Hector storm generally capture the same chemical features within the cloud as the model simulation run with the observed flash rates (Fig. 22). All three cross-sections show NO_x values in excess of 3 ppbv between 7-8 km in altitude, with a slight enhancement from 13-14 km. However, when maximum vertical velocity is selected as the storm parameter to predict flash rates the resulting NO_x mixing ratios at 13:25 LT exceed 3 ppbv between 5-14 km. This larger vertical range of enhanced NO_x (Fig. 22c) is likely due to the distribution of LNO_x produced by the large spike in flash rates around ~13:05 LT (Fig. 21). The corresponding vertical cross-sections of model O_3 from the selected FRPSs at 13:25 LT indicate the O_3 mixing ratios (Fig. 23 left) reflect the slight differences in NO_x within the storm cloud (Fig. 22). A larger area of 13-16 ppbv model O_3 covers a greater horizontal distance (~30 km) between 6-14 km in altitude in the cross-sections where flash rates are predicted using storm parameters, especially maximum vertical velocity (Fig. 23b left). More O_3 titration would occur at times when a greater presence of NO_x, due to increased lightning, is present within the model storm. The similarity in the O_3 cross-sections at 13:35 LT (Fig. 23 right) is likely due to the increase in observed flash rates and the decrease in predicted flash rates from the storm parameters around 13:40 LT (Fig. 21). These trends in flash rate would allow more O_3 titration to occur within the model simulation using lightning observations and less within the model simulations using the selected storm parameters.

6 Conclusions

The 3-D WRF-AqChem model produces an idealized Hector storm with many characteristics similar to those observed. Cloud top height, horizontal dimensions of the convective cell and

anvil, and peak radar reflectivity are roughly within 3%, 17%, and 8% of the observations, respectively. Generally, the Hector storm evolution in the model is 2 hours ahead of the observed storm. Mean anvil-level simulated CO and NO_x, when a lightning NO production scenario of 500 moles NO $flash^{-1}$ is used, compare well with Egrett observations, although the results for CO show a small overestimate in upward convective transport to anvil levels. However, this transport overestimate, uncertainty in the placement of the upper mode for IC LNO_x production, and the lack of Egrett anvil observations in more than one model layer, led to the possibility that LNO_x production per flash could have been as large as 600 moles. Future improvements to the LNO_x parameterization to inject the NO_x for individual flashes along specific channels would likely improve the simulated NO_x frequency distribution in the anvil. The Geophysica NO_x observations suggest the upper tropospheric peak in lightning channel segments may occur 1-3 km higher in altitude than assumed in the model. Approximately 85% of the total LNO_x mass resided above 7 km in the later stages of the storm. Small decreases in O_3 in the region of peak lightning NO production are noted, likely from chemical loss involving titration by fresh NO emissions.

The mean NO production per flash for midlatitude and subtropical events previously studied with a similar approach is roughly equivalent to the results presented for this Hector storm. Analyses of aircraft NO_x observations and flash data from other tropical regions (e.g., Brazil, West Africa) suggest smaller NO production per flash in the tropics than in midlatitudes (Huntrieser et al., 2008; Huntrieser et al., 2011). Aircraft observations of another Hector storm from SCOUT-O3/ACTIVE also showed larger NO_x production per flash than in other tropical events. The upper tropospheric column NO_2 computed from the Hector simulation is of similar magnitude to that computed from midlatitude and subtropical simulations (Ott et al., 2010) and

greater than in the tropical marine events observed by OMI (Bucsela et al., 2010). Therefore, we conclude that Hector, and other tropical island convection, may not be representative of other types of tropical thunderstorms. The wind velocity difference between the anvil outflow and steering level of the Hector storm was less than for most midlatitude storms, but the directional difference was significant in Hector, which could lead to enhanced flash length. However, additional research is required to further assess the Huntrieser et al. (2008) hypothesis that more LNO_x may be produced per stroke in storms with greater wind shear. The use of FRPSs within a cloud-resolved simulation in the tropics also indicates that for the 16 November 2005 Hector storm, maximum vertical velocity and cloud top height are two modeled storm parameters that generally capture the observed lightning flash rate trend and associated NO_x production, given the proper scaling factors are applied.

Acknowledgements

This research was supported under NASA Aura Validation Program funding provided to Dr. Kenneth Pickering. The National Center for Atmospheric Research is supported by the National Science Foundation. The ACTIVE project was supported by the UK Natural Environment Research Council, grant NE/C512688/1 and directed by Geraint Vaughan of the University of Manchester. I would like to thank my advisor Dr. Kenneth Pickering for his guidance, support, and feedback during this research, as well as Tabitha Huntemann for her initial work and contributions to setting up and running this Hector thunderstorm simulation. I would also like to thank Heidi Huntrieser from Deutsches Zentrum für Luft- und Raumfahrt for her comments.

References

Allen, G., Vaughan, G., Bower, K. N., Williams, P. I., Crosier, J., Flynn, M., Connolly, P., Hamilton, J. F., Lee, J. D., Saxton, J. E., Watson, N. M., Gallagher, M., Coe, H., Allan, J., Choularton, T. W., and Lewis, A. C.: Aerosol and trace-gas measurements in the Darwin area during the wet season, J. Geophys. Res., 113, D06306, doi:10.1029/2007JD008706, 2008.

Barth, M. C., Kim, S.-W., Skamarock, W. C., Stuart, A. L., Pickering, K. E., and Ott, L. E.: Simulations of the redistribution of formaldehyde, formic acid, and peroxides in the 10 July 1996 Stratospheric-Tropospheric Experiment: Radiation, Aerosols, and Ozone deep convection storm, J. Geophys. Res., 112, D13310, doi:10.1029/2006JD008046, 2007a.

Barth, M. C., Kim, S.-W., Wang, C., Pickering, K. E., Ott, L. E., Stenchikov, G., Leriche, M., Cautenet, S., Pinty, J.-P., Barthe, C., Mari, C., Helsdon, J. H., Farley, R. D., Fridlind, A. M., Ackerman, A. S., Spiridonov, V., and Telenta, B.: Cloud-scale model intercomparison of chemical constituent transport in deep convection, Atmos. Chem. Phys., 7, 4709-4731, 2007b, www.atmos-chem-phys.net/7/4709/2007/.

Barthe, C., Pinty, J.-P., and Mari, C.: Lightning-produced NO_x in an explicit electrical scheme tested in a Stratosphere-Troposphere Experiment: Radiation, Aerosols, and Ozone case study, J. Geophys. Res., 112, D04302, doi:10.1029/2006JD007402, 2007.

Barthe, C., and Barth, M. C.: Evaluation of a new lightning-produced NO_x parameterization for cloud resolving models and its associated uncertainties, Atmos. Chem. Phys., 8, 4691-4710, 2008.

Barthe, C., Deierling, W., and Barth, M. C.: Estimation of total lightning from various storm parameters: A cloud-resolving model study, J. Geophys. Res., 115, D24202, doi:10.1029/2010JD014405, 2010.

Beirle, S., Salzmann, M., Lawrence, M. G., and Wagner, T.: Sensitivity of satellite observations for freshly produced lightning NO_x, Atmos. Chem. Phys., 9, 1077-1094, doi:10.5194/acp-9-1077-2009, 2009.

Beirle, S., Huntrieser, H., and Wagner, T.: Direct satellite observations of lightning-produced NOx, Atmos. Chem. Phys, 10, 10965-10986, doi:10.5194/acp-10-10965-2010, 2010.

Betz, H.-D., Schmidt, K., Oettinger, W. P., and Wirz, M.: Lightning detection with 3D-discrimination of intracloud and cloud-to-ground discharges, Geophys. Res. Lett., 31, L11108, doi:10.1029/2004GL019821, 2004.

Betz, H.-D., Schmidt, K., Fuchs, B., Oettinger, W. P., and Höller, H.: Cloud lightning: Detection and utilization for total lightning measured in the VLF/LF regime, J. Lightning Res., 2, 1-17, 2007.

Betz, H.-D., Schmidt, K., and Oettinger, W. P.: LINET – An International VLF/LF Lightning Detection Network in Europe, in: Lightning: Principles, Instruments and Applications, Eds. H.-D. Betz, U. Schumann, and P. Laroche, Springer, Dordrecht (NL), Ch. 5, 2008.

Boersma, K. F., Eskes, H. J., Meijer, E. W., and Kelder, H. M.: Estimates of lightning NOx production from GOME satellite observations, Atmos. Chem. Phys., 5, 2311-2331, doi:10.5194/acp-5-2311-2005, 2005.

Brunner, D., Siegmund, P., May, P. T., Chappel, L., Schiller, C., Miller, R., Peter, T., Fueglistaler, S., MacKenzie, A. R., Fix, A., Schlager, H., Allen, G., Fjaeraa, A. M., Streibel, M., and Harris, N. R. P.: The SCOUT-O3 Darwin Aircraft Campaign: rationale and meteorology, Atmos. Chem. Phys., 9 93-117, 2009, www.atmos-chem-phys.net/9/93/2009/.

Bucsela, E. J., Pickering, K. E., Huntemann, T. L., Cohen, R. C., Perring, A., Gleason, J. F., Blakeslee, R. J., Albrecht, R. I., Holzworth, R., Cipriani., J. P., Vargar-Navarro, D., Mora-Segura, I., Pacheco-Hernandez, A., and Laporte-Molina, S.: Lightning-generated NO_x seen by the Ozone Monitoring Instrument during NASA's Tropical Composition, Cloud and Climate Coupling Experiment (TC^4), J. Geophys. Res., 115, D00J10, doi:10.1029/2009JD013118, 2010.

Carbone, R. E., Keenan, T. D., Hacker, J., and Wilson, J. W.: Tropical island convection in the absence of significant topography. Part I: Life cycle of diurnally forced convection. Mon. Wea. Rev., 128, 3459-3480, 2000.

Chatfield, R. B., and Crutzen, P. J.: Sulfur dioxide in remote ocean air: Cloud transport of reactive precursors, J. Geophys. Res., 89, 7111-7132, 1984.

Chemel, C., Russo, M. R., Pyle, J. A., Sokhi, R. S., and Schiller, C.: Quantifying the imprint of a severe Hector thunderstorm during ACTIVE/SCOUT-O3 onto the water content in the upper troposphere/lower stratosphere, Mon. Wea. Rev., 137, 2493-2514, doi:10.1175/2008MWR2666.1, 2009.

Crook, N. A.: Understanding Hector: the dynamics of island thunderstorms, Mon. Wea. Rev., 129, 1550-1563, 2001.

Dahl, J. M. L., Höller, H., and Schumann, U.: Modeling the flash rate of thunderstorms. Part I: Framework, Mon. Wea. Rev., 139, 3093-3111, doi:10.1175/MWR-D-10-05031.1, 2011a.

Dahl, J. M. L., Höller, H., and Schumann, U.: Modeling the flash rate of thunderstorms. Part II: Implementation, Mon. Wea. Rev., 139, 3112-3124, doi:10.1175/MWR-D-10-05032.1, 2011b.

DeCaria, A. J., Pickering, K. E., Stenchikov, G. L., Scala, J. R., Stith, J. L., Due, J. E., Ridley, B. A., and Laroce, P.: A cloud-scale model study of lightning-generated NO_x in an individual thunderstorm during STERAO-A, J. Geophys. Res., 105, 11601 – 11616, 2000.

DeCaria, A. J., Pickering, K.E., Stenchikov, G. L., and Ott, L. E.: Lightning-generated NO_x and its impact on tropospheric ozone production: A 3-D modeling study of a STERAO-A thunderstorm, J. Geophys. Res., 110, D14303, doi:10.1029/2004JD005556, 2005.

Deierling, W., and Petersen, W. A.: Total lightning activity as an indicator of updraft characteristics, J. Geophys. Res., 113, D16210, doi:10.1029/2007JD009598, 2008.

Deierling, W., Petersen, W. A., Latham, J., Ellis, S., and Christian, H. J.: The relationship between lightning activity and ice fluxes in thunderstorms, J. Geophys. Res., 113, D15210, doi:10.1029/2007JD009700, 2008.

Dickerson, R. R., Huffman, G. J., Luke, W. T., Nunnermacker, L. J., Pickering, K. E., Leslie, A. C. D., Lindsey, C. G., Slinn, W. G. N., Kelly, T. J., Daum, P. H., Delany, A. C., Greenberg, J. P., Zimmerman, P. R., Boatman, J. F., Ray, J. D., and Steadman, D. H.: Thunderstorms: An important mechanism in the transport of air pollutants, Science, 235, 460-465, 1987.

Fehr, T., Höller, H., and Huntrieser, H.: Model study on production and transport of lightning-produced NO_x in a EULINOX supercell storm, J. Geophys. Res., 109, D09102, doi:10.1029/2003JD003935, 2004.

Golding, B. W.: A numerical investigation of tropical island thunderstorms, Mon. Wea. Rev., 121, 1417-1433, 1993.

Höller, H., Betz, H.-D., Schmidt, K., Calheiros, R. V., May, P., Houngninou, E., and Scialom, G.: Lightning characteristics observed by a VLF/LF lightning detection network (LINET) in Brazil, Australia, Africa and Germany, Atmos. Chem. Phys., 9, 7795-7824, 2009, www.atmos-chem-phys.net/9/7795/2009/.

Huntrieser, H., Schlager, H., Roiger, A., Lichtenstern, M., Schumann, U., Kurz, C., Brunner, D., Schwierz, C., Richter, A., and Stohl, A.: Lightning-produced NO_x over Brazil during TROCCINOX: airborne measurements in tropical and subtropical thunderstorms and the importance of mesoscale convective systems, Atmos. Chem. Phys., 7, 2987-3013, 2007, www.atmos-chem-phys.net/7/2987/2007/.

Huntrieser, H., Schumann, U., Schlager, H., Höller, H., Giez, A., Betz, H.-D., Brunner, D., Forster, C., Pinto Jr., O., and Calheiros, R.: Lightning activity in Brazilian thunderstorms during TROCCINOX: implications for NO_x production, Atmos. Chem. Phys., 8, 921-953, 2008, www.atmos-chem-phys.net/8/921/2008/.

Huntrieser, H., Schlager, H., Lichtenstern, M., Roiger, A., Stock, P., Minikin, A., Höller, H., Schmidt, K., Betz, H.-D., Allen, G., Viciani, S., Ulanovsky, A., Ravegnani, F., and Brunner, D.: NO_x production by lightning in Hector: first airborne measurements during SCOUT-O3/ACTIVE, Atmos. Chem. Phys., 9, 8377-8412, 2009, www.atmos-chem-phys.net/9/8377/2009/.

Huntrieser, H., Schlager, H., Lichtenstern, M., Stock, P., Hamburger, T., Höller, H., Schmidt, K., Betz, H.-D., Ulanovsky, A., et al.: Mesoscale convective systems observed during AMMA and their impact on the NO_x and O_3 budget over West Africa, Atmos. Chem. Phys., 11, doi:10.5194/acp-11-2503-2011, 2011.

Isaac, P., and Hacker, J.: ACTIVE VH-ARA data set, ARA Technical Report, Airborne Research Australia/Finders University, Salisbury South, Australia, 106 pp., 2007.

IPCC: Climate Change 2007: The Physical Science Basis. Contribution of Working Group I to the Fourth Assessment Report of the Intergovernmental Panel on Climate Change, Eds. Solomon, S., Qin, D., Manning, M., Chen, Z., Marquis, M., Averyt, K. B., Tignor, M., and Miller, H. L., Cambridge, United Kingdom and New York, NY, USA, pp. 996, 2007.

Koike, M., Kondo, Y., Kita, K., Takegawa, N., Nishi, N., Kashihara, T., Kawakami, S., Kudoh, S., Blake, D., Shirai, T., Liley, B., Ko, M., Miyazaki, Y., Kawasaki, Z., and Ogawa, T.: Measurements of reactive nitrogen produced by tropical thunderstorms during BIBLE-C, J. Geophys. Res., 112, D18304, doi:10.1029/2006JD008193, 2007.

Kuhlman, K. M., MacGorman, D. R., Biggerstaff, M. I., and Krehbiel, P. R.: Lightning initiation in the anvils of two supercell storms, Geophys. Res. Lett., 36, L07802, doi:10.1029/2008GL036650, 2009.

Labrador, L. J., von Kuhlmann, R., and Lawrence, M. G.: The effects of lightning-produced NO_x and its vertical distribution on atmospheric chemistry: sensitivity simulations with MATCH-MPIC, Atmos. Chem. Phys., 5, 1815-1834, 2005, www.atmos-chem-phys.org/acp/5/1815/.

Labrador, L., Vaughan, G., Heyes, W., Waddicor, D., Volz-Thomas, A., Pätz, H.-W., and Höller, H.: Lightning-produced NO_x during the Northern Australian monsoon; results from the ACTIVE campaign, Atmos. Chem. Phys., 9, 7419–7429, 2009, www.atmos-chem-phys.net/9/7419/2009/.

Lang, S. E., Tao, W.-K., Zeng, X., and Li, Y.: Reducing the biases in simulated radar reflectivities from a bulk microphysics scheme: Tropical convective systems, J. Atmos. Sci., 68, 2306-2320, 2011.

Lin, Y.-L., Farley, R. D., and Orville, H. D.: Bulk parameterization of the snow field in a cloud model, J. Clim. Appl. Meteorol., 22, 1065-1092, 1983.

MacGorman, D. R., and W. D. Rust, The Electrical Nature of Storms, 422 pp., Oxford Univ. Press, New York, 1998.

Madronich, S., and Flocke, S.: The role of solar radiation in atmospheric chemistry, in Handbook of Environmental Chemistry, Eds. P. Boule, Springer, New York, 1-26, 1999.

May, P. T., and Ballinger, A.: The statistical characteristics of convective cells in a monsoon regime (Darwin, Northern Australia), Mon. Wea. Rev., 135, 82-92, doi:10.1175/MWR3273.1, 2007.

McCaul, E. W., Goodman, S. J., LaCasse, K. M., and Cecil, D. J.: Forecasting lightning threat using cloud-resolving model simulations, Weather Forecast., 24, doi:10.1175/2008WAF2222152.1, 2009.

Ott, L. E., Pickering, K. E., Stenchikov, G. L., Huntrieser, H., and Schumann, U.: Effects of lightning NO_x production during the 21 July European Lightning Nitrogen Oxides Project storm studied with a three-dimensional cloud-scale chemical transport model, J. Geophys. Res., 112, D05307, doi:10.1029/2006JD007365, 2007.

Ott, L. E., Pickering, K. E., Stenchikov, G. L., Allen, D. J., DeCaria, A. J., Ridley, B., Lin, R.-F., Wang, D., Lang, S., and Tao, W.-K.: Production of lightning NO_x and its vertical distribution calculated from 3-D cloud-scale chemical transport model simulations, J. Geophys. Res., 115, D04301, doi:10.1029/2009JD011880, 2010.

Petersen, W. A., Christian, H. J., and Rutledge, S. A.: TRMM observations of the global relationship between ice water content and lightning, Geophys. Res. Lett., 32, L14819, doi:10.1029/2005GL023236, 2005.

Pickering, K. E., Thompson, A. M., Dickerson, R. R., Luke, W. T., and McNamara, D. P.: Model calculations of tropospheric ozone production potential following observed convective events, J. Geophys. Res., 95, 14049-14062, 1990.

Pickering, K. E., Thompson, A. M., Scala, J. R., Tao, W.-K., Dickerson, R. R., and Simpson, J.: Free tropospheric ozone production following entrainment of urban plumes into deep convection, J. Geophys. Res., 97, 17985-18000, 1992.

Pickering, K. E., Thompson, A. M., Tao, W., and Kucsera, T. L.: Upper tropospheric ozone production following mesoscale convection during STEP/EMEX, J. Geophys. Res., 98, 8737-8749, 1993.

Pickering, K. E., Wang, Y., Tao, W.-K., Price, C., and Müller, J.-F.: Vertical distribution of lightning NO_x for use in regional and global chemical transport models, J. Geophys. Res., 103, 31203-31216, 1998.

Price, C., and Rind, D.: A simple lightning parameterization for calculating global lightning distributions, J. Geophys. Res., 97, 9919-9933, doi:10.1029/92JD00719, 1992.

Price, C., and Rind, D.: What determines the cloud-to-ground lightning fraction in thunderstorms?, Geophys. Res. Lett., 20, 463-466, 1993.

Price, C., Penner, J., and Prather, M.: NO_x from lightning 1. Global distribution based on lightning physics, J. Geophys. Res., 102, 5929-5941, 1997.

Saito, K., Keenan, T., Holland, G., and Puri, K.: Numerical simulation of the diurnal evolution of tropical island convection over the Maritime Continent, Mon. Wea. Rev., 129, 378-400, 2001.

Salzmann, M., Lawrence, M. G., Phillips, V. T. J., and Donner, L. J.: Cloud resolving model study of the roles of deep convection for photo-chemistry in the TOGA COARE/CEPEX region, Atmos. Chem. Phys., 8, 2741-2757, 2008.

Schumann, U., and Huntrieser, H.: The global lightning-induced nitrogen oxides source, Atmos. Chem. Phys., 7, 3823-3907, www.atmos-chem-phys.net/7/3823/2007/, 2007.

Seidel, D. J., Ross, R. J., Angell, J. K., and Reid, G. C.: Climatological characteristics of the tropical tropopause as revealed by radiosondes, J. Geophys. Res., 106, 7857-7878, doi:10.1029/2000JD900837, 2001.

Skamarock, W. C., Klemp, J. B., Dudhia, J., Gill, D., Barker, D., Wang, W., and Powers, J. G.: A description of the Advanced Research WRF Version 2., Technical Note NCAR/TN-468+STR, NCAR, Boulder, Colorado, 2005.

Vaughan, G., Schiller, C., MacKenzie, A. R., Bower, K., Peter, T., Schlager, H., Harris, N. R. P., and May, P. T.: SCOUT-O3/ACTIVE: High-altitude aircraft measurements around deep tropical convection, Bull. Amer. Meteor. Soc., 89, 647–662, 2008.

Wang, C., and Prinn, R.: On the roles of deep convective clouds in tropospheric chemistry, J. Geophys. Res., 105(D17), 22269-22298, 2000.

Zhang, X., Helsdon Jr., J. H., and Farley, R. D.: Numerical modeling of lightning-produced NO_x using an explicit lightning scheme: 1. Two-dimensional simulation as a "proof of concept", J. Geophys. Res., 108(D18), 4579, doi:10.1029/2002JD003224, 2003a.

Zhang, X., Helsdon Jr., J. H. , and Farley, R. D.: Numerical modeling of lightning-produced NO_x using an explicit lightning scheme: 2. Three-dimensional simulation and expanded chemistry, J. Geophys. Res., 108(D18), 4580, doi:10.1029/2002JD003225, 2003b.

Table 1. Summary of cloud-resolved simulations of LNO_x production.

Model	Moles NO per CG flash	P_{IC}/P_{CG}	Field Campaign	Region	Reference
2-D GCE	200-500	> 0.5	STERAO-A	Midlatitude	DeCaria et al. (2000)
3-D GCE/CSCTM	460	0.75-1.00	STERAO-A	Midlatitude	DeCaria et al. (2005)
MM5	330	1.4	EULINOX	Midlatitude	Fehr et al. (2004)
3-D GCE/CSCTM	360	1.15	EULINOX	Midlatitude	Ott et al. (2007)
3-D GCE/MM5/ CSCTM	500 +	0.94 +	STERAO-A; EULINOX; CRYSTAL-FACE	3 midlatitude; 2 subtropical	Ott et al. (2010)
Intercomparison *	36-465	~0.1-1.0	STERAO-A	Midlatitude	Barth et al., (2007b)

+ indicates that the value is a mean value based on five storm simulations; * Intercomparison of six models simulating LNO_x; GCE: Goddard Cumulus Ensemble model; CSCTM: Cloud-Scale Chemical Transport Model; MM5: Penn State/NCAR Mesoscale Model version 5; STERAO-A: Stratosphere-Troposphere Experiment: Radiation, Aerosols and Ozone; EULINOX: European Lightning Nitrogen Oxides Project; CRYSTAL-FACE: Cirrus Regional Study of Tropical Anvils and Cirrus Layers – Florida Area Cirrus Experiment

Table 2. Six FRPSs incorporated into the cloud-resolved model simulation.

Type of FRPS	Equation (flashes min^{-1})	Reference
Maximum vertical velocity	$5.7 \times 10^{-6} \times w_{max}^{4.5}$	Price and Rind (1992)
Cloud top height	$3.44 \times 10^{-5} H^{4.9}$	Price and Rind (1992)
Updraft volume	$6.75 \times 10^{-11} w_5$ - 13.9	Deierling and Petersen (2008)
Ice water path	$33.33 \times IWP$ - 0.17	Petersen et al. (2005)
Precipitation ice mass	$3.4 \times 10^{-8} p_m$ - 18.1	Deierling et al. (2008)
Ice mass flux product	$9.0 \times 10^{-15} (f_p \times f_{np})$ + 13.4	Deierling et al. (2008)

Table 3. Summary of the observed and simulated features in the 16 November 2005 Hector thunderstorm.

	Observations	**Simulation**
Initial radar indication of cell at 2.5 km	14:28 LT	11:55 LT
Initial anvil development at 13 km	15:03 LT	12:55 LT
Peak radar reflectivity at 2.5 km	16:00 LT (~60 dBZ)	14:15 LT (~65 dBZ)
Initial anvil dissipation at 13 km	18:03 LT	16:15 LT
Complete cell dissipation at 2.5 km	18:28 LT	15:55 LT

Table 4. Egrett observed and simulated CO mixing ratio statistics for the layer centered at 13.4 km. Simulated values are based on a lightning NO production scenario of 450 and 500 moles flash^{-1}. The layer centered at 13.4 km contained 351 11-second Egrett observations and 1268 simulated values.

	Initial Condition CO (ppbv)	**Observed Anvil CO (ppbv)**	**Simulated Anvil CO (ppbv)**	
			450 moles NO flash^{-1}	**500 moles NO flash^{-1}**
Mean	70.1	84.0	86.9	85.8
Maximum	---	114.5	117.4	117.4
Standard Deviation	---	9.9	15.3	14.8

Table 5. Statistics for the Egrett observed NO_x mixing ratios for the layer centered at 13.4 km compared with the simulated NO_x mixing ratios for the layers centered at 12.0 km and 12.7 km. Simulated values are based on a lightning NO production scenario of 450 and 500 moles $flash^{-1}$. The layer centered at 13.4 km contained 338 11-second Egrett observations and the layers centered at 12.0 km (12.7 km) contained 2236 (1782) simulated values.

450 moles NO $Flash^{-1}$				
	Initial Condition NO_x (pptv)	**Observed Anvil NO_x (pptv)**	**Simulated Anvil NO_x (pptv)**	
			12.0 km	**12.7 km**
Mean	140	845	758	739
Maximum	---	5139	2678	2606
Standard Deviation	---	1140	692	602

500 moles NO $Flash^{-1}$				
	Initial Condition NO_x (pptv)	**Observed Anvil NO_x (pptv)**	**Simulated Anvil NO_x (pptv)**	
			12.0 km	**12.7 km**
Mean	140	845	834	811
Maximum	---	5139	2970	2889
Standard Deviation	---	1140	769	670

Table 6. Statistics for the Geophysica observed and simulated tracer mixing ratios for multiple layers centered at 11.4-16.6 km. Simulated values are based on a lightning NO production scenario of 500 moles flash^{-1}.

Altitude (km)	# Obs	Mean CO (ppbv)		Maximum CO (ppbv)		CO Standard Deviation (ppbv)	
		Observed	Simulated	Observed	Simulated	Observed	Simulated
11.4	1	67.6	90.5	67.6	117.0	--	10.8
12.0	11	66.1	93.8	67.4	124.5	0.6	10.4
12.7	20	68.6	91.0	71.4	123.3	1.0	11.8
13.4	33	67.9	85.8	74.5	117.4	4.0	15.3
14.1	43	65.1	80.8	68.2	118.0	1.9	18.1
14.9	42	66.0	75.3	72.2	122.9	4.7	20.7
15.7	66	70.3	65.8	75.5	126.4	4.9	19.1
16.6	32	59.3	63.0	63.9	124.6	2.7	15.2

Altitude (km)	# Obs	Mean NO_x (pptv)		Maximum NO_x (pptv)		NO_x Standard Deviation (pptv)	
		Observed	Simulated	Observed	Simulated	Observed	Simulated
11.4	0	--	639	--	2840	--	700
12.0	4	10	834	13	2970	4	769
12.7	20	476	811	922	2889	258	670
13.4	16	984	705	3028	2745	967	617
14.1	30	2826	587	3363	2540	621	604
14.9	38	597	475	1654	2248	548	534
15.7	52	162	364	243	2036	31	408
16.6	32	94	432	118	1760	7	283

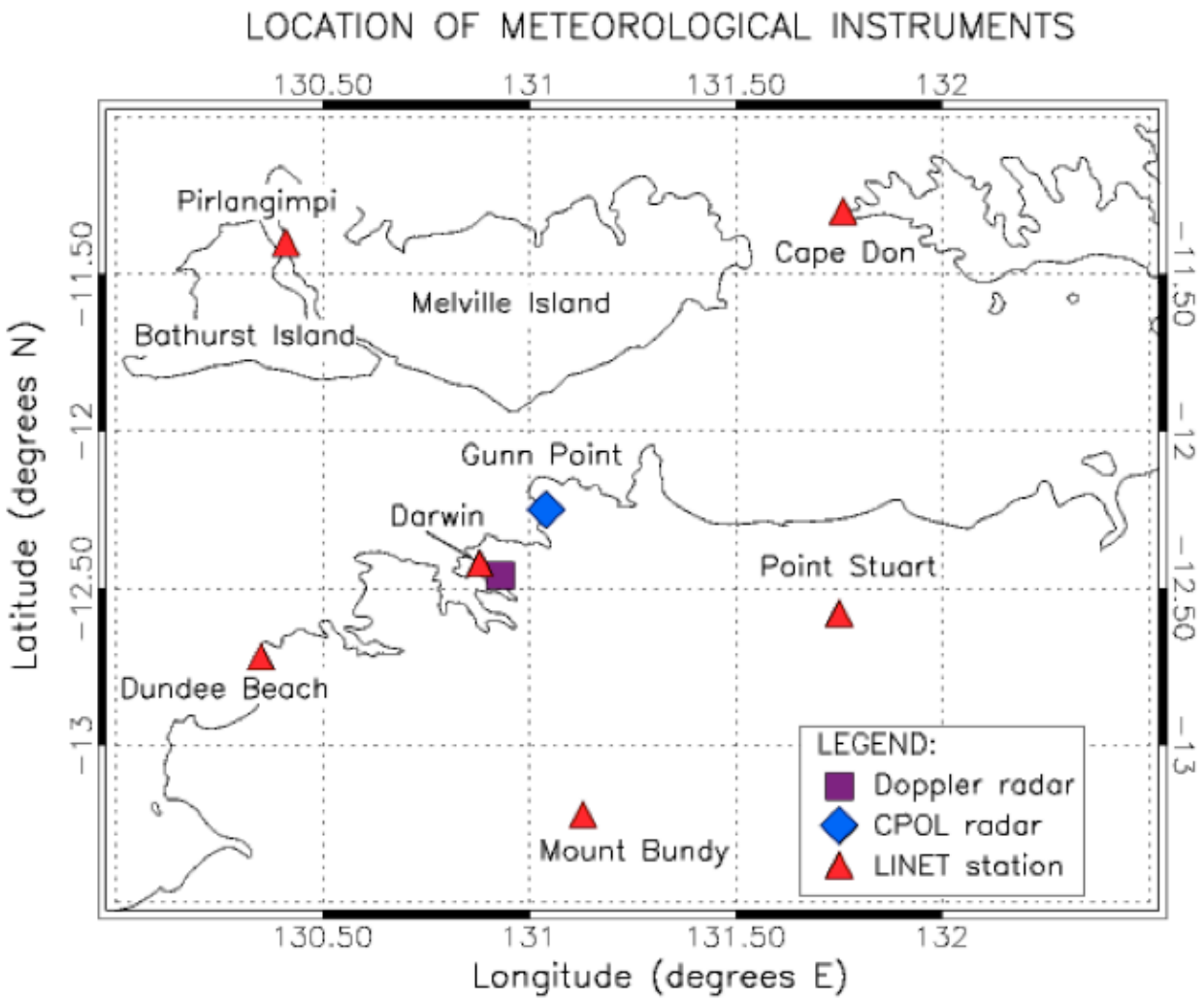

Figure 1. Location of the two CAWCR radar and six LINET stations involved in the campaign.

Figure 2. Development of the Hector thunderstorm over the Tiwi Islands on 16 November 2005 during the SCOUT-O3/ACTIVE field campaign. From left to right, the photos indicate the stage of single-cell development at ~16:19 LT and ~17:09 LT, respectively.

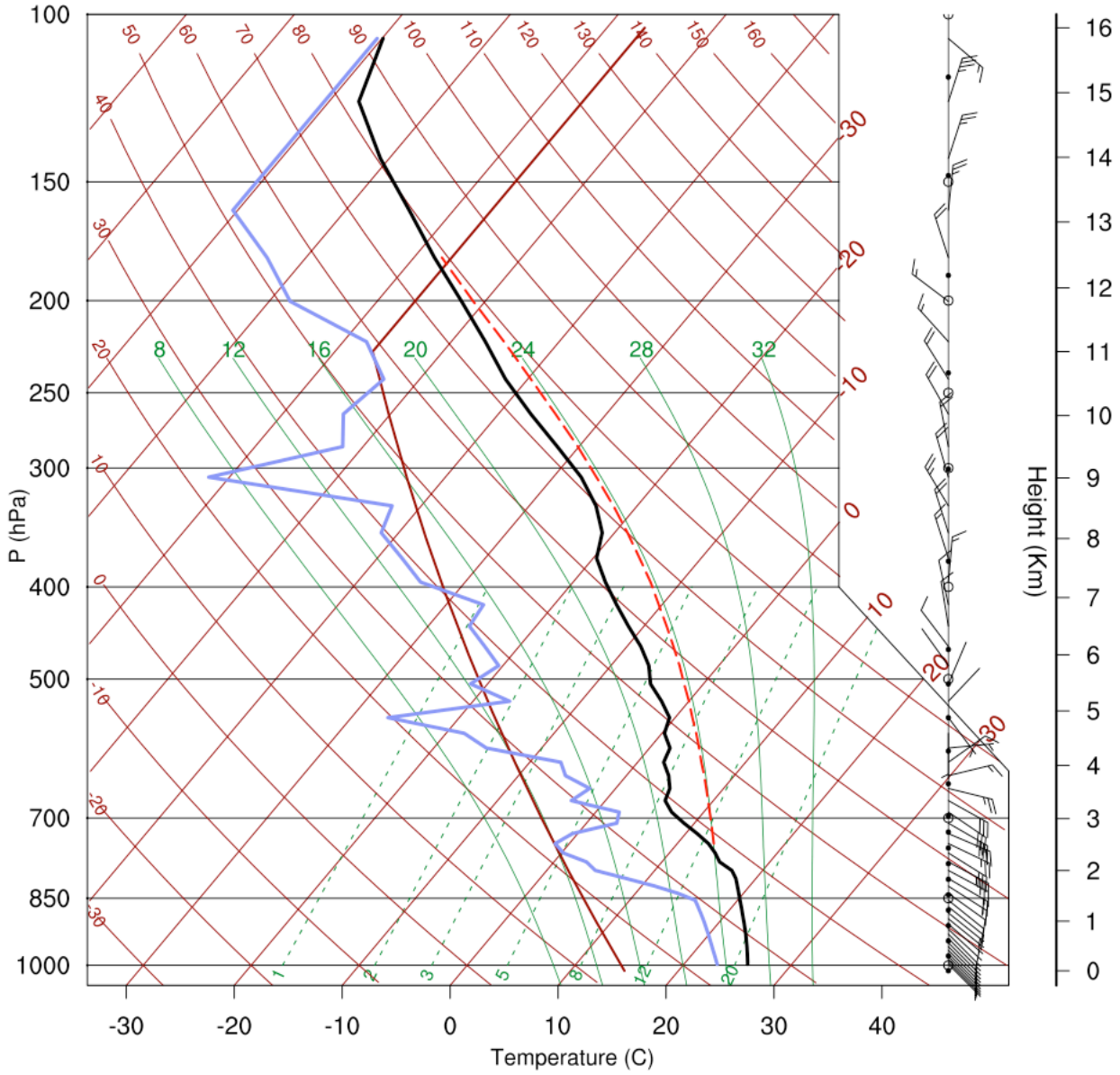

Figure 3. Sounding used in the horizontally-homogeneous simulation initialization. Temperature and dew point are plotted as black and blue lines, respectively. Wind speed is reported in knots, where a full barb is equivalent to 10 knots.

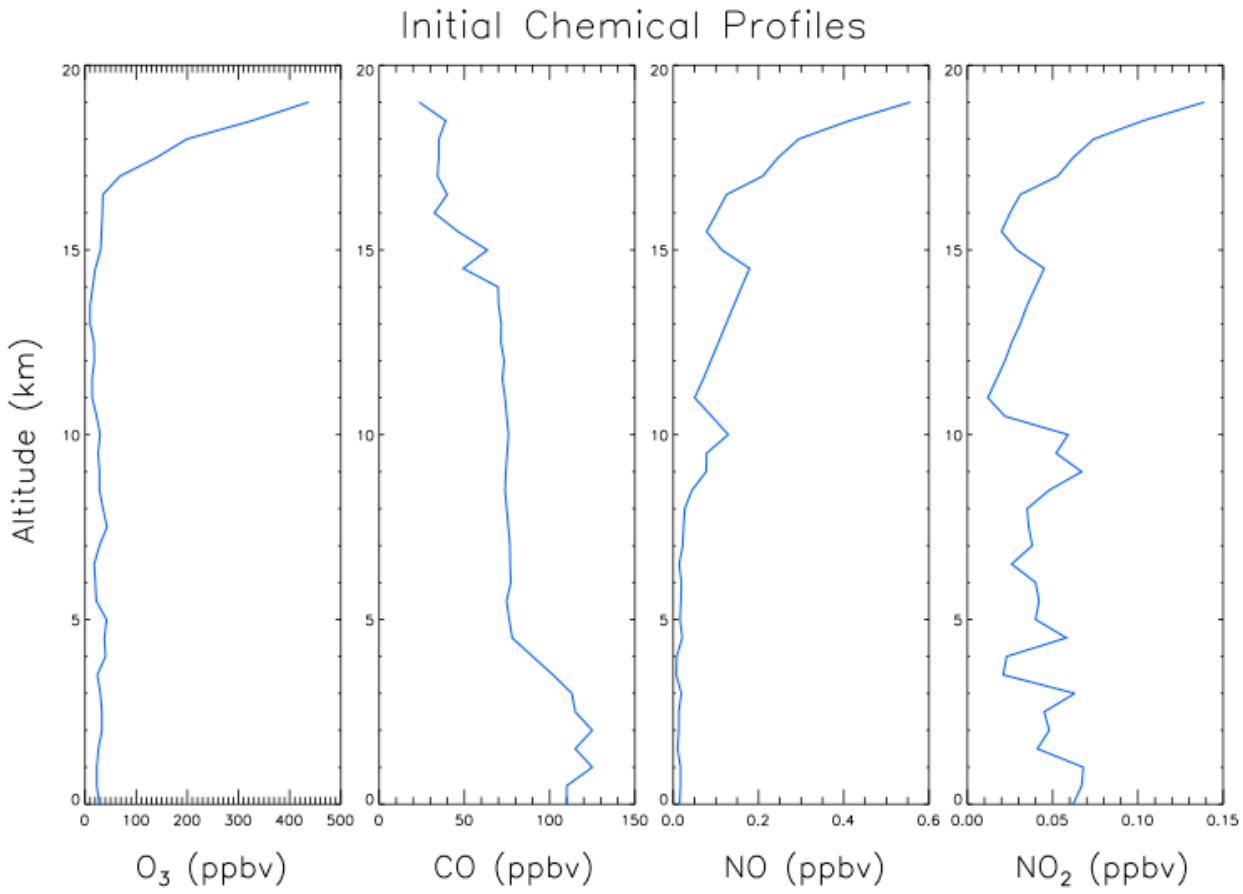

Figure 4. Initial chemical profiles based on composite of Dornier, Falcon, Geophysica, and Egrett measurements.

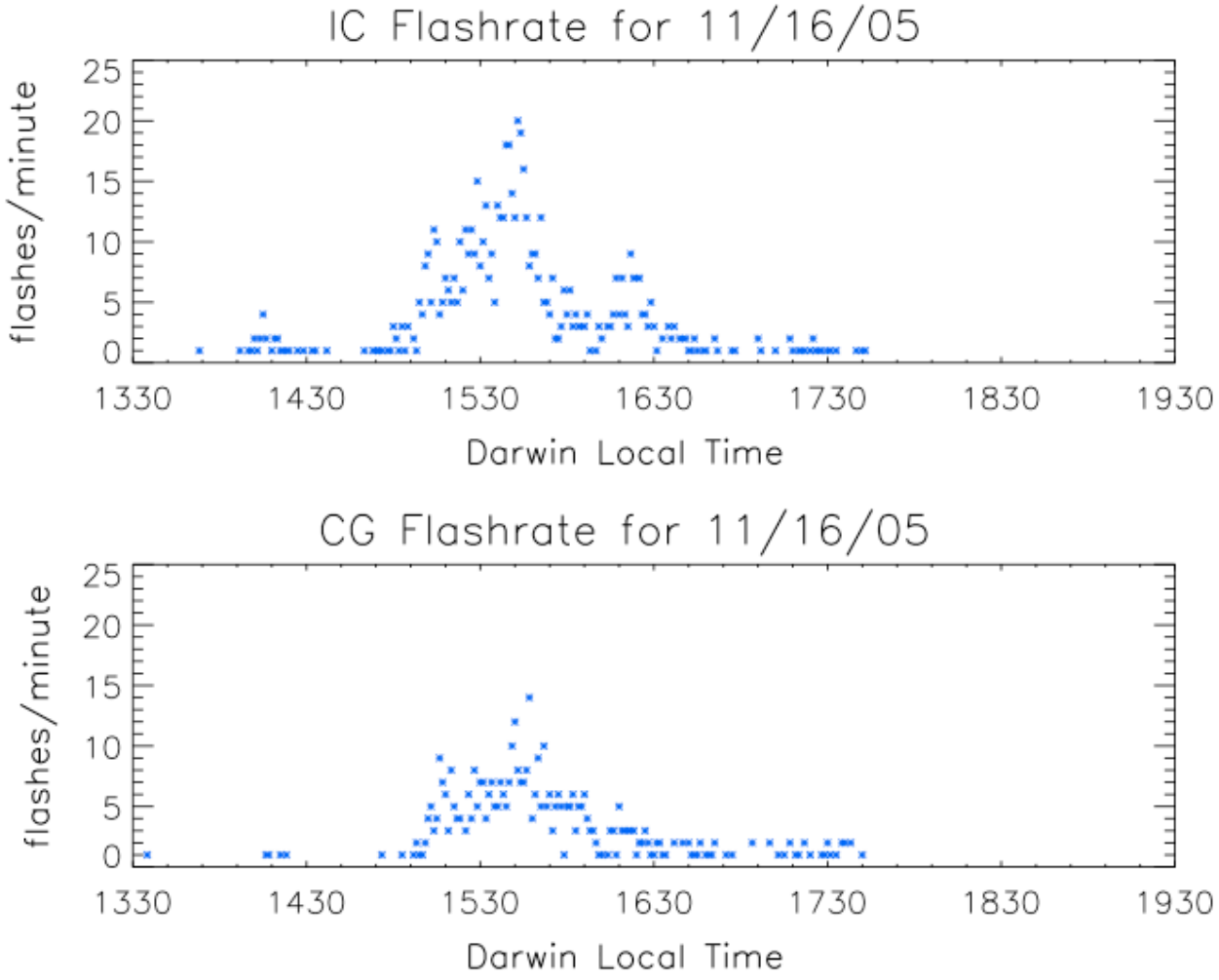

Figure 5. Time series of IC and CG flashes per minute for 13:30 – 19:30 LT for the selected Hector storm.

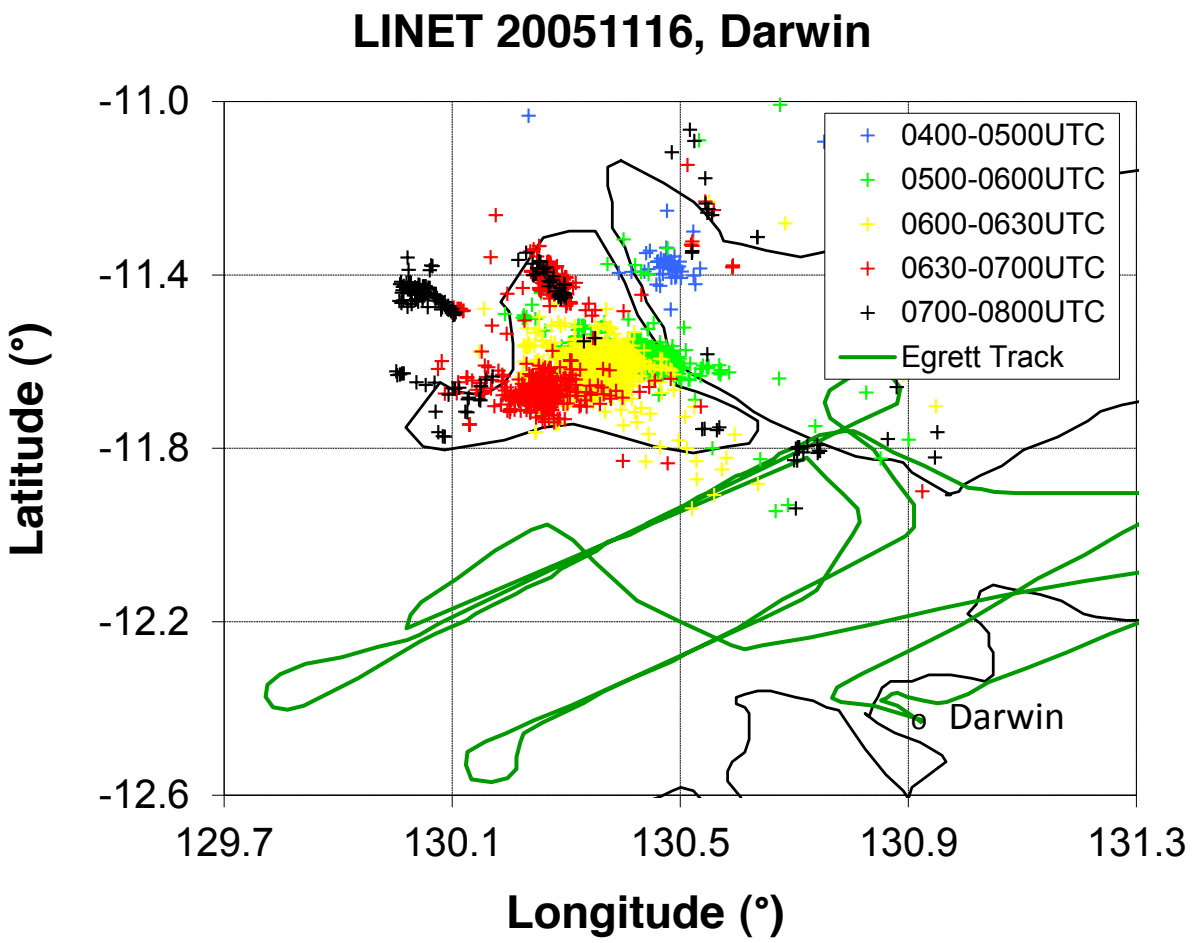

Figure 6. Lightning strokes (CG and IC) observed by LINET on 16 November 2005 for the Hector thunderstorm that tracked across the Tiwi Islands between roughly 14:30-18:30 LT (05:00-09:00 UTC). The solid green line represents an approximation of the Egrett flight track through the anvil between 06:28-09:47 UTC (Isaac and Hacker, 2007).

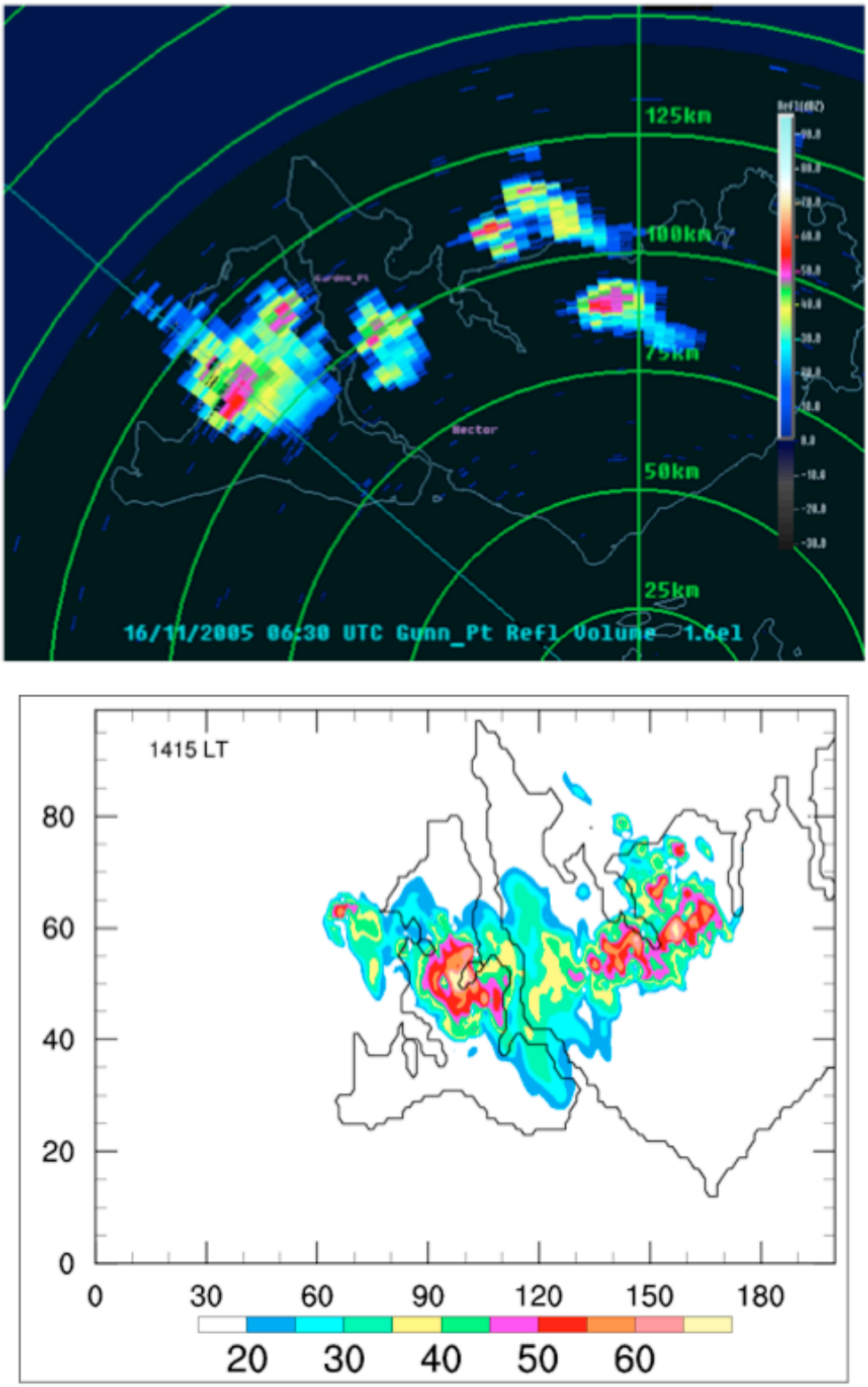

Figure 7. Comparison of observed radar reflectivity at 16:00 LT (top, from Vaughan et al., 2008) to modeled 2.5 km reflectivity at 14:15 LT (bottom). Note the radar echo intensity (dBZ) in the observed radar reflectivity (top) is contoured at every 10 dBZ with the red/magenta interface approximating 50 dBZ. The X and Y axes in the bottom figure show distance in km.

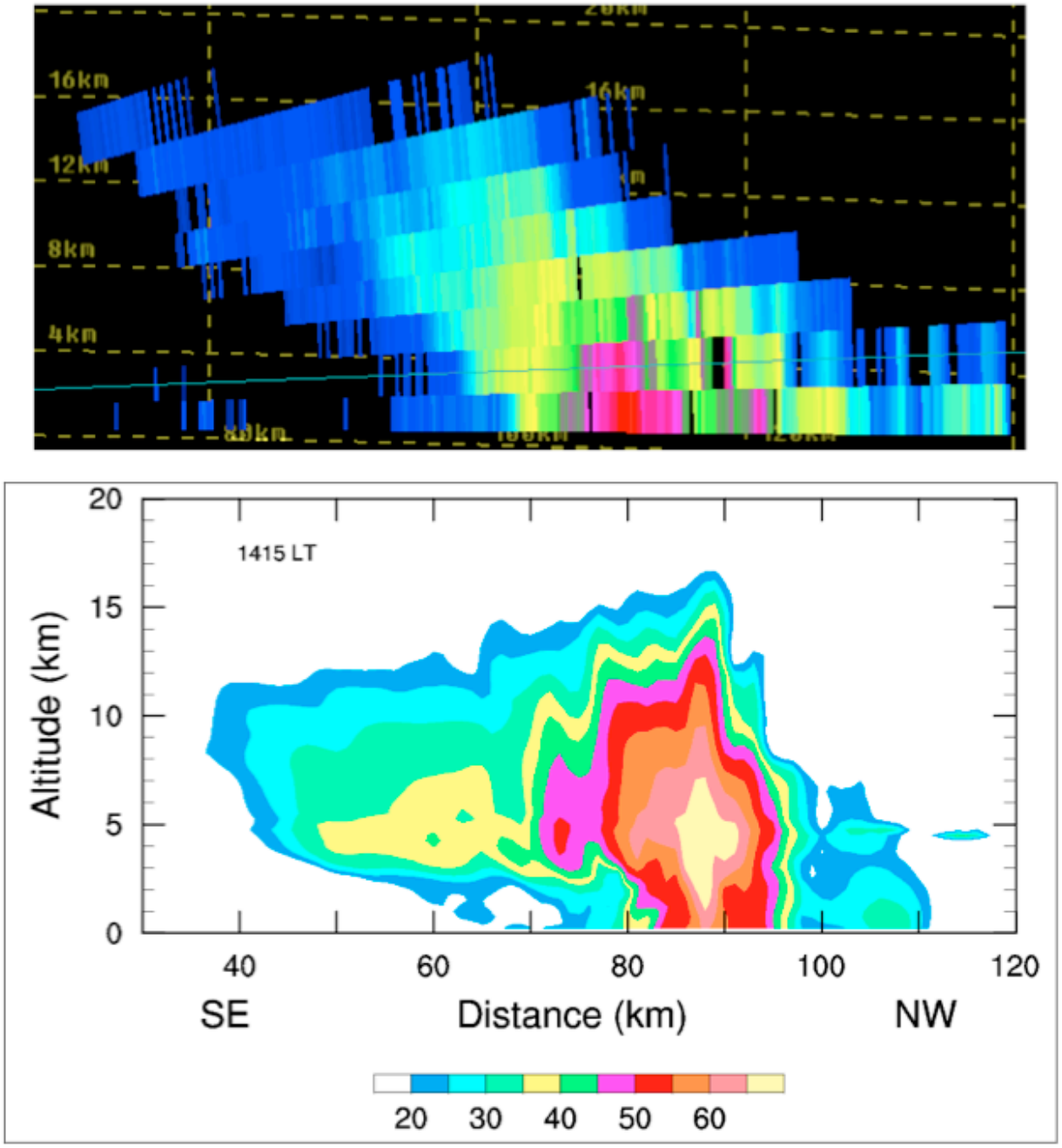

Figure 8. Vertical cross section comparison of observed radar reflectivity at 16:00 LT (top, from Vaughan et al., 2008) to modeled reflectivity at 14:15 LT (bottom). The radar echo density (dBZ) is contoured in both vertical cross sections. Note that the observed radar reflectivity follows the same dBZ scaling as Fig. 7 (top).

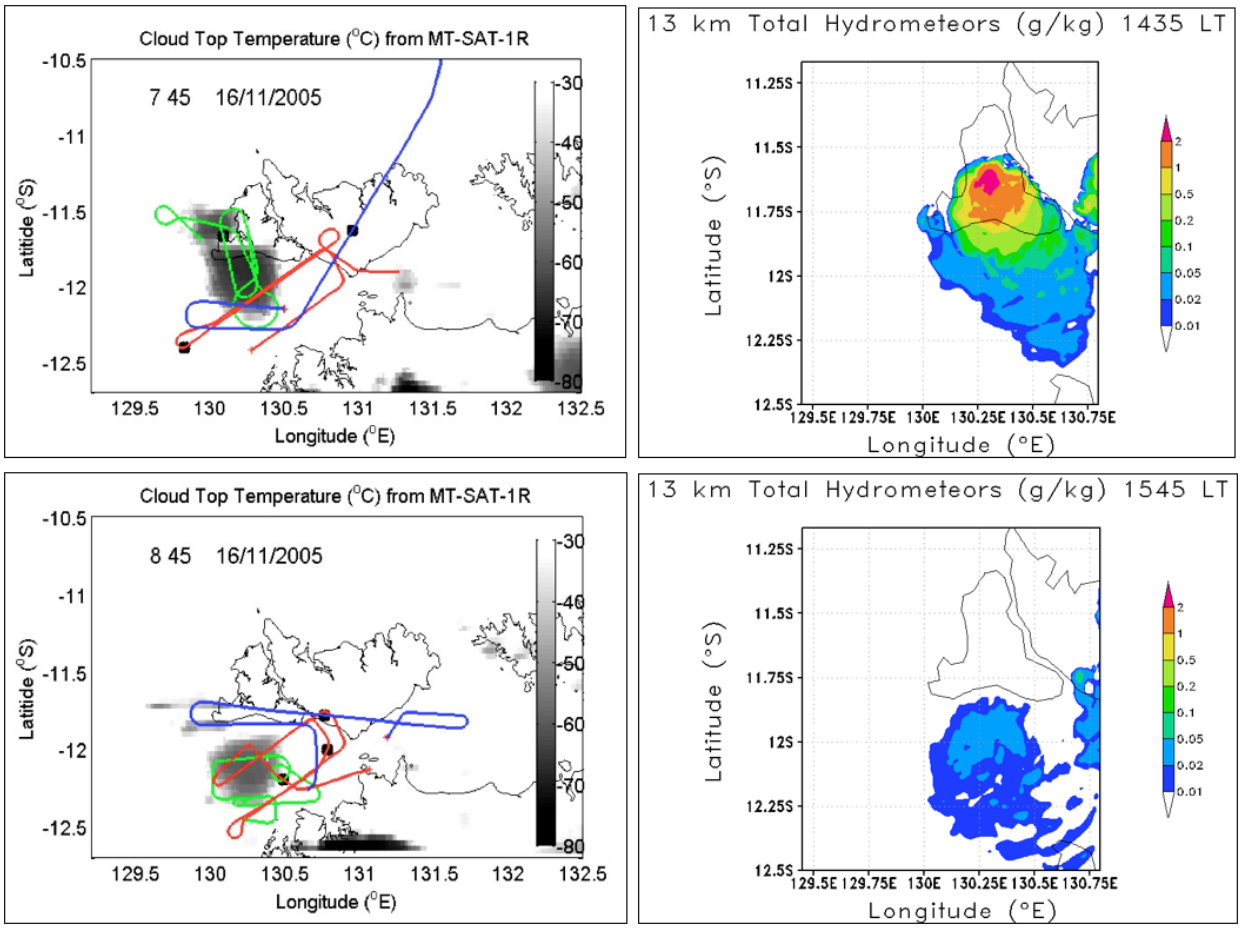

Figure 9. Comparison of IR satellite anvil observations and aircraft flight tracks (left) with modeled total hydrometeors at 13 km (right). A summation of the area containing simulated total hydrometeors ≥ 0.01 g kg^{-1} provides an estimate of the anvil extent. Egrett flight track is in red, Geophysica in green, and Falcon in blue.

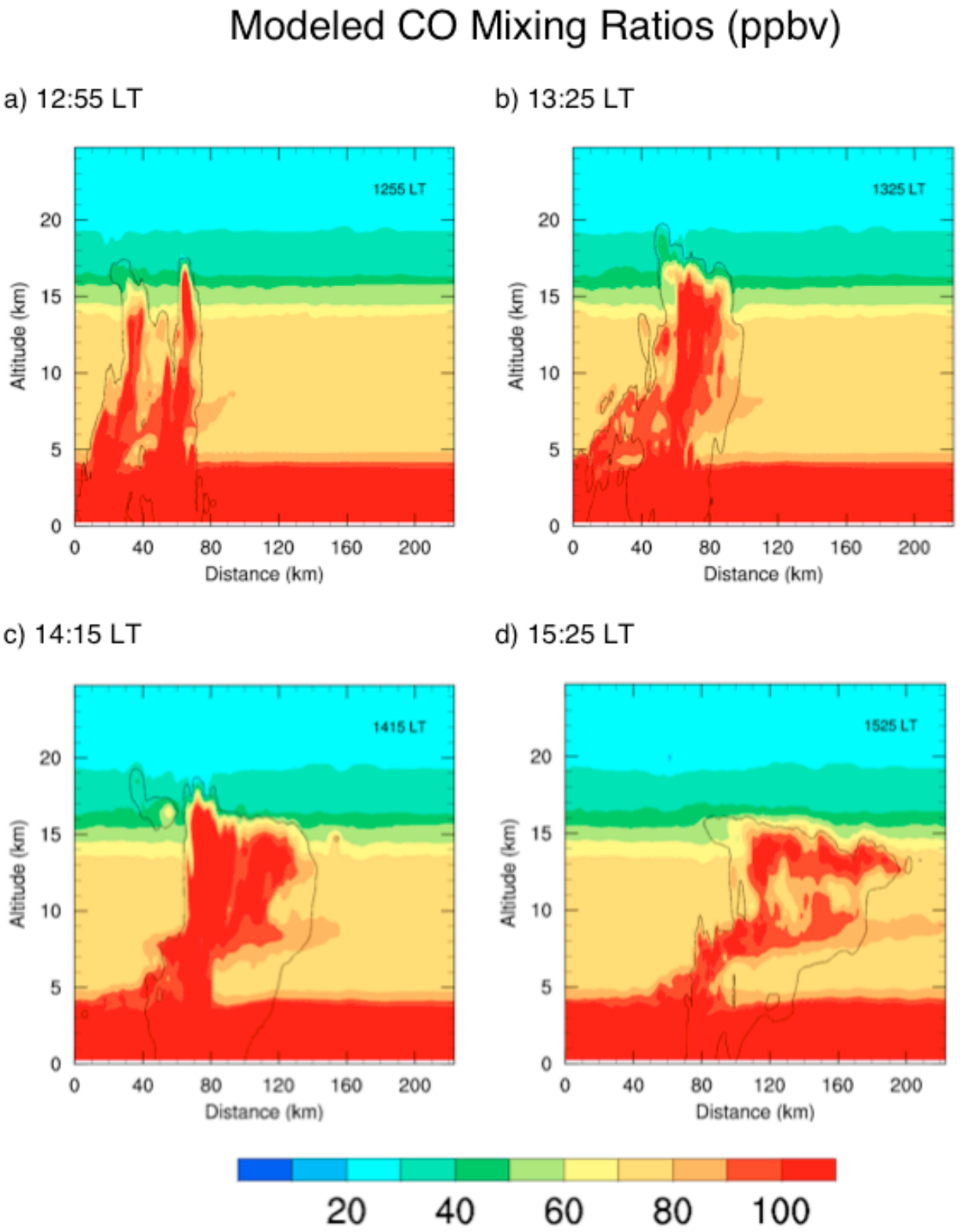

Figure 10. Time series of vertical cross sections of CO mixing ratios from times (a) 12:55 LT, (b) 13:25 LT, (c) 14:15 LT, (d) 15:25 LT, oriented 130° from north through the storm core. The thin black line indicates the 0.01 g kg^{-1} total condensate contour.

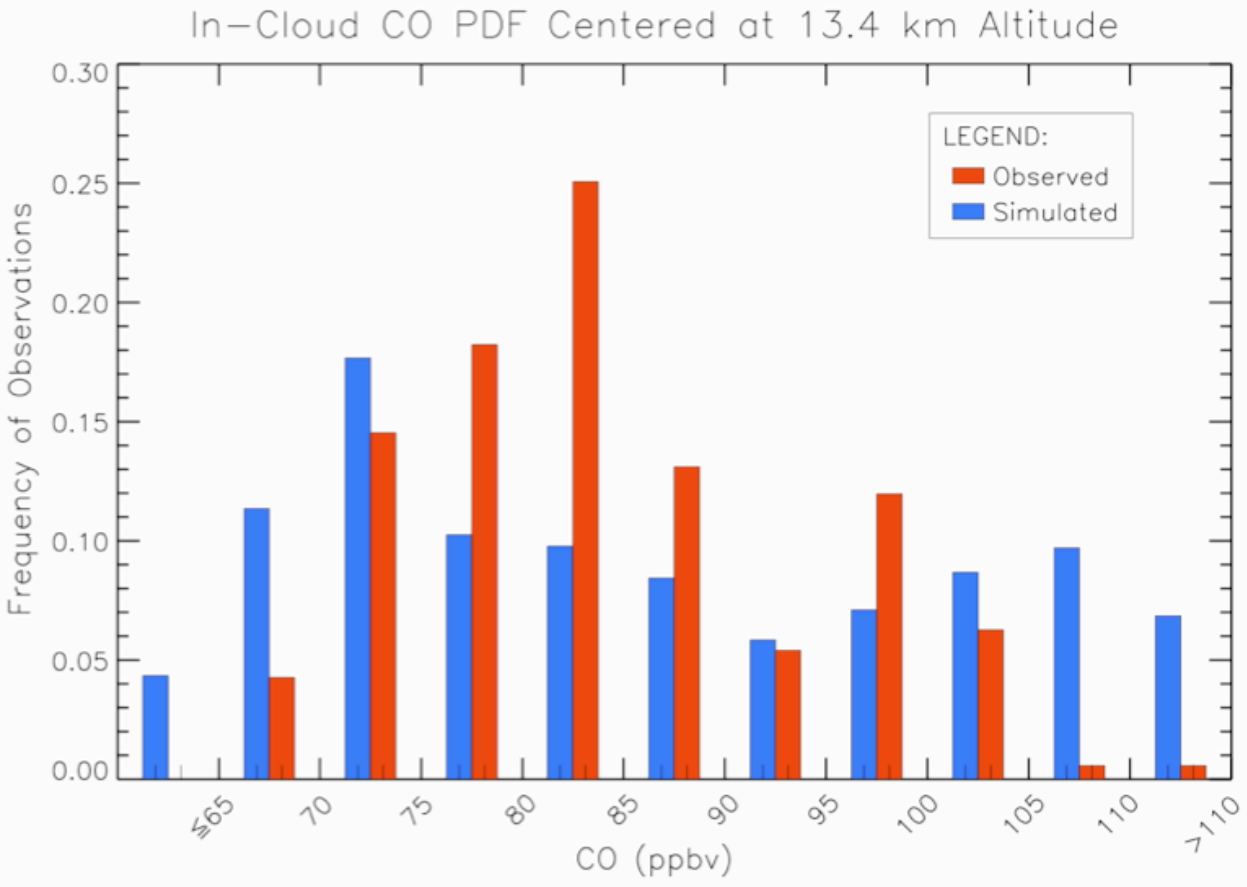

Figure 11. PDF of observed Egrett (red) and simulated (blue) CO mixing ratios in the model layers centered at 13.4 km given 500 moles NO flash^{-1}.

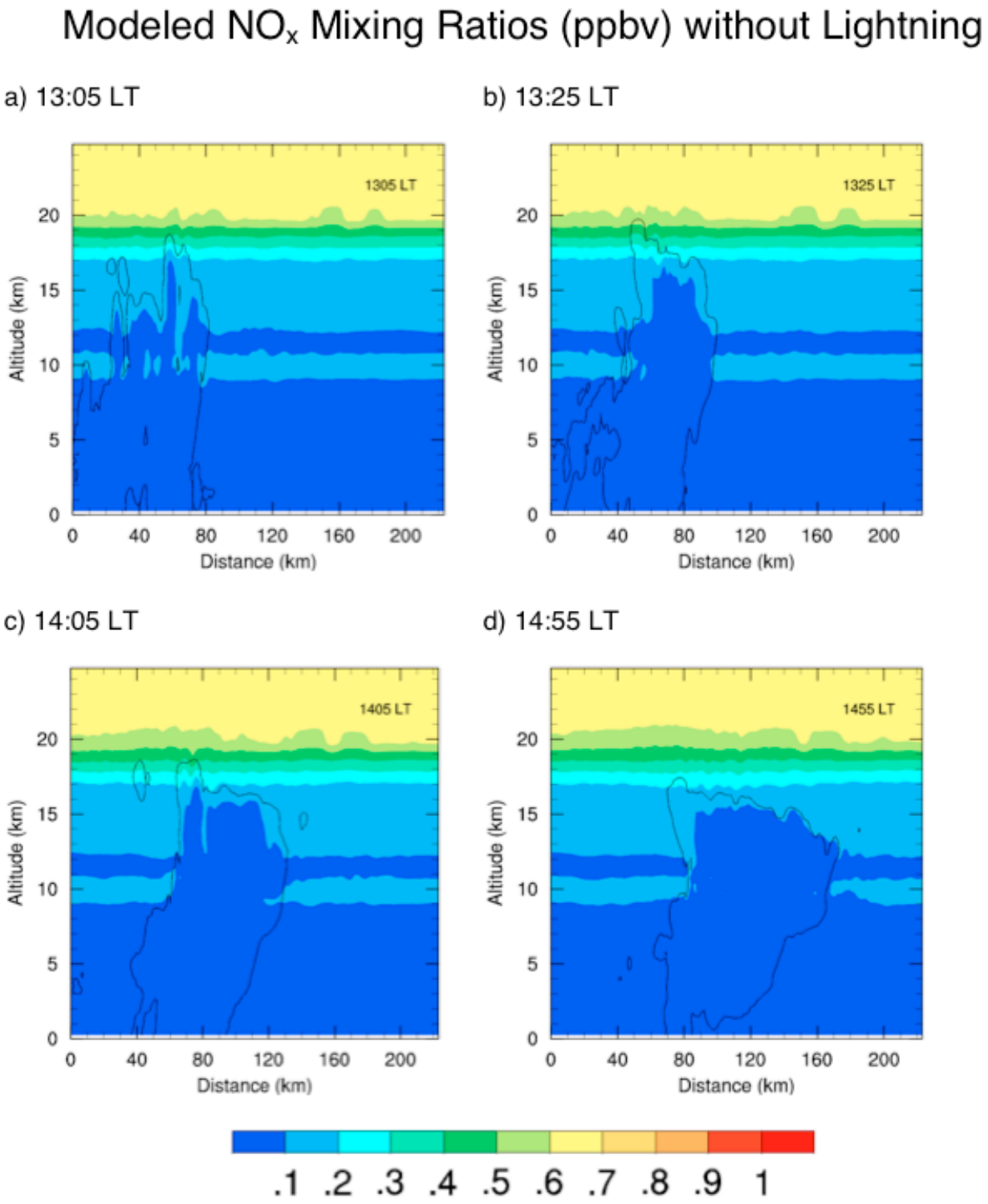

Figure 12. Time series of vertical cross sections of NO_x mixing ratios for simulations without lightning NO production at a) 13:05 LT, b) 13:25 LT, c) 14:05 LT, and d) 14:55 LT, oriented 130º from north through the storm core. The thin black line indicates the 0.01 g kg^{-1} total condensate contour.

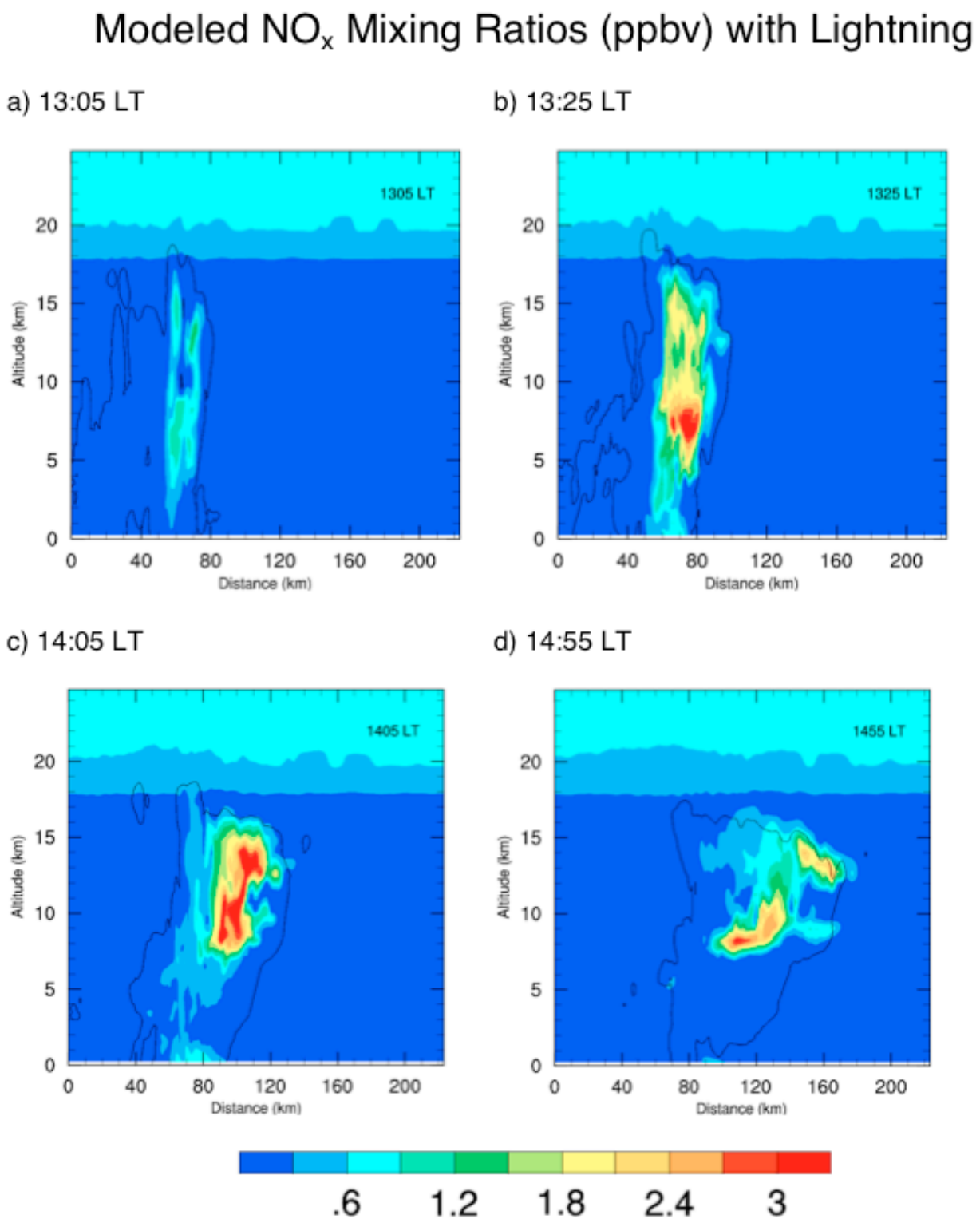

Figure 13. Time series of vertical cross sections of NO_x mixing ratios for simulations with lightning NO production of 500 moles flash^{-1} at a) 13:05 LT, b) 13:25 LT, c) 14:05 LT, and d) 14:55 LT, oriented 130º from north through the storm core. The thin black line indicates the 0.01 g kg^{-1} total condensate contour.

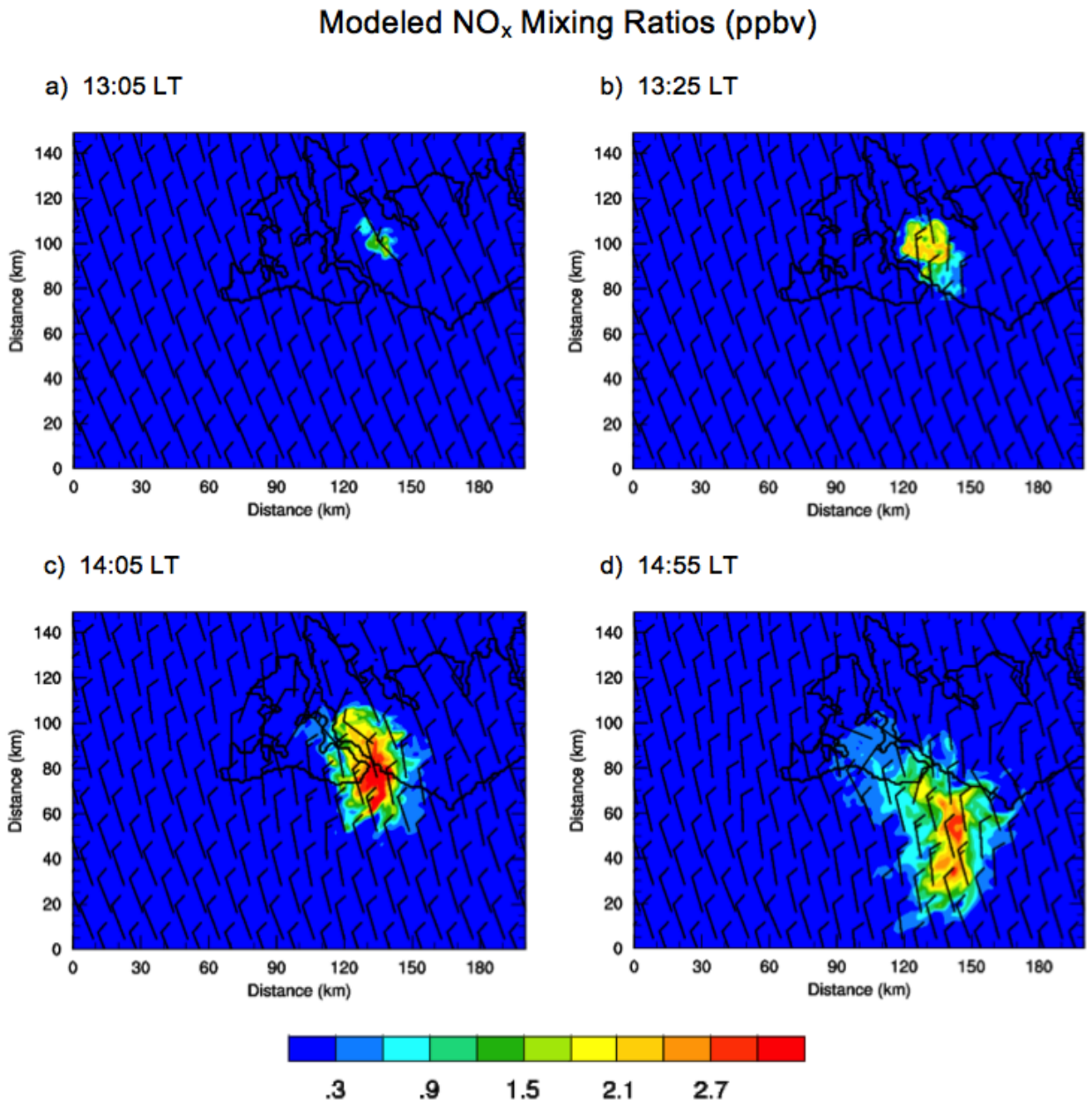

Figure 14. Time series of NO_x mixing ratios at 13 km for simulations with lightning NO production of 500 moles flash^{-1} at a) 13:05 LT, b) 13:25 LT, c) 14:05 LT, and d) 14:55 LT. Arrows indicate wind vectors at 13 km. Wind speed is reported in m s^{-1}, where a full barb is equivalent to 10 m s^{-1}.

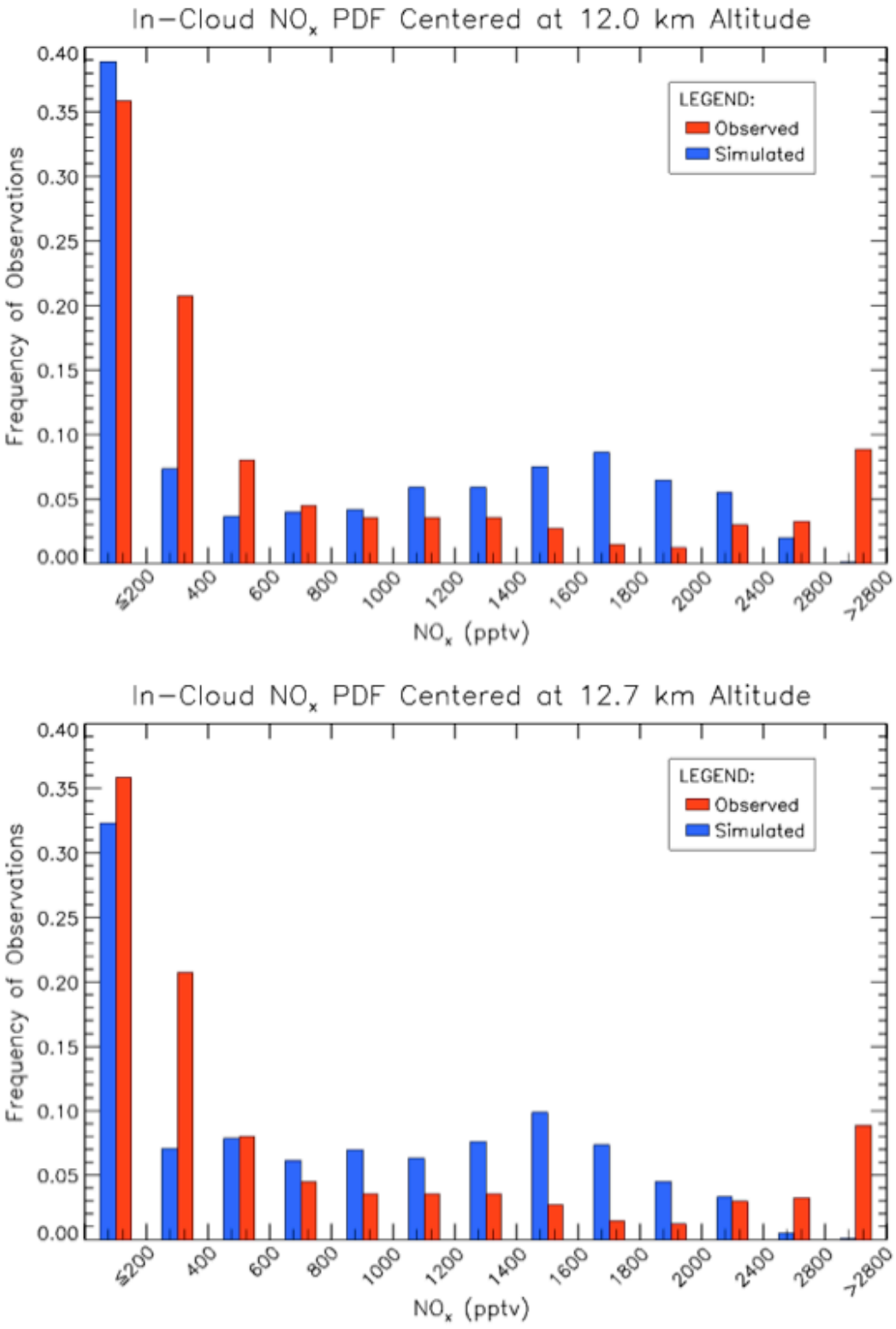

Figure 15. PDF of NO_x mixing ratios estimated from Egrett observations (red) and simulated (blue) in the model layer centered at 12.0 km and 12.7 km given 500 moles NO flash^{-1}. The Egrett observed NO_x includes the directly measured NO_x between 13.2-13.8 km and that estimated from the photostationary state when only one of NO or NO_2 were available.

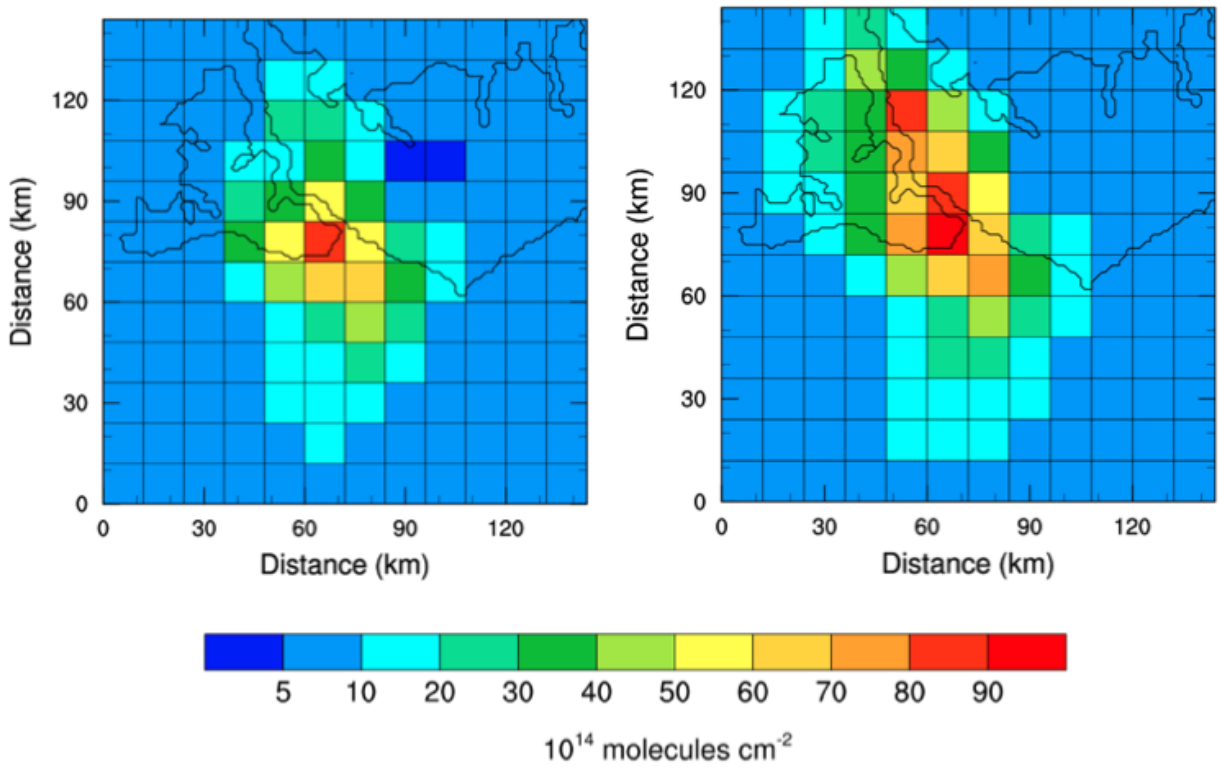

Figure 16. Partial NO_2 columns from the tropopause (105 mb) to 400 mb (left) and 600 mb (right) for the simulated Hector thunderstorm at 14:45 LT. Each column covers 12 × 12 km^2 area. The tropopause height is estimated based on the idealized sounding and the climatological mean pressure of the lapse-rate tropopause from radiosonde data (Seidel et al., 2001).

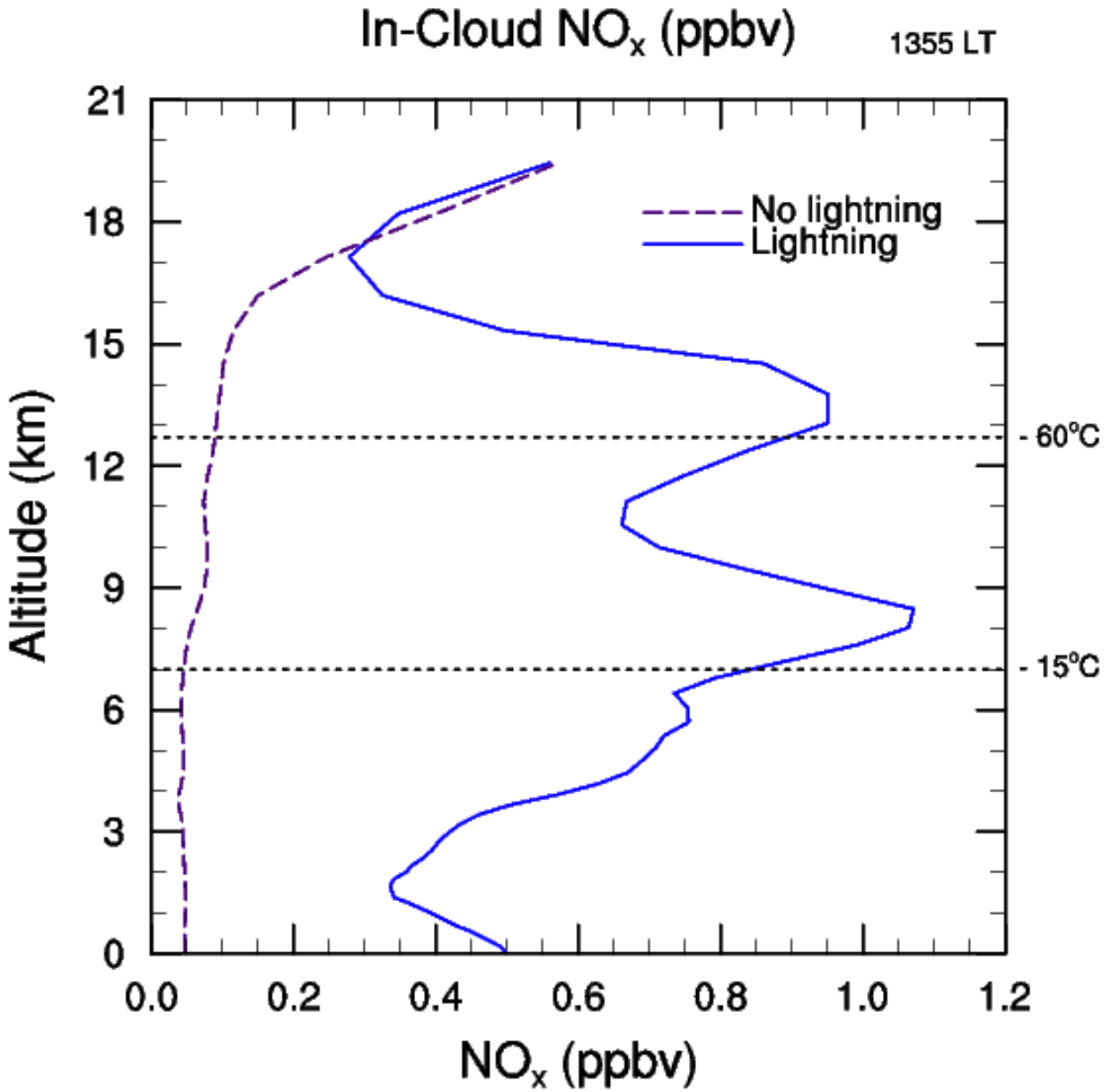

Figure 17. Average in-cloud NO_x at 13:55 LT for model simulations with and without lightning. Above 17.1 km, values represent the average NO_x directly above the cloud at 17.1 km for model simulations with and without lightning. The dashed lines at 7.0 and 12.7 km represent the usual altitude of the isotherms used for the lower and upper modes, respectively, of the vertical distribution of the lightning NO_x source.

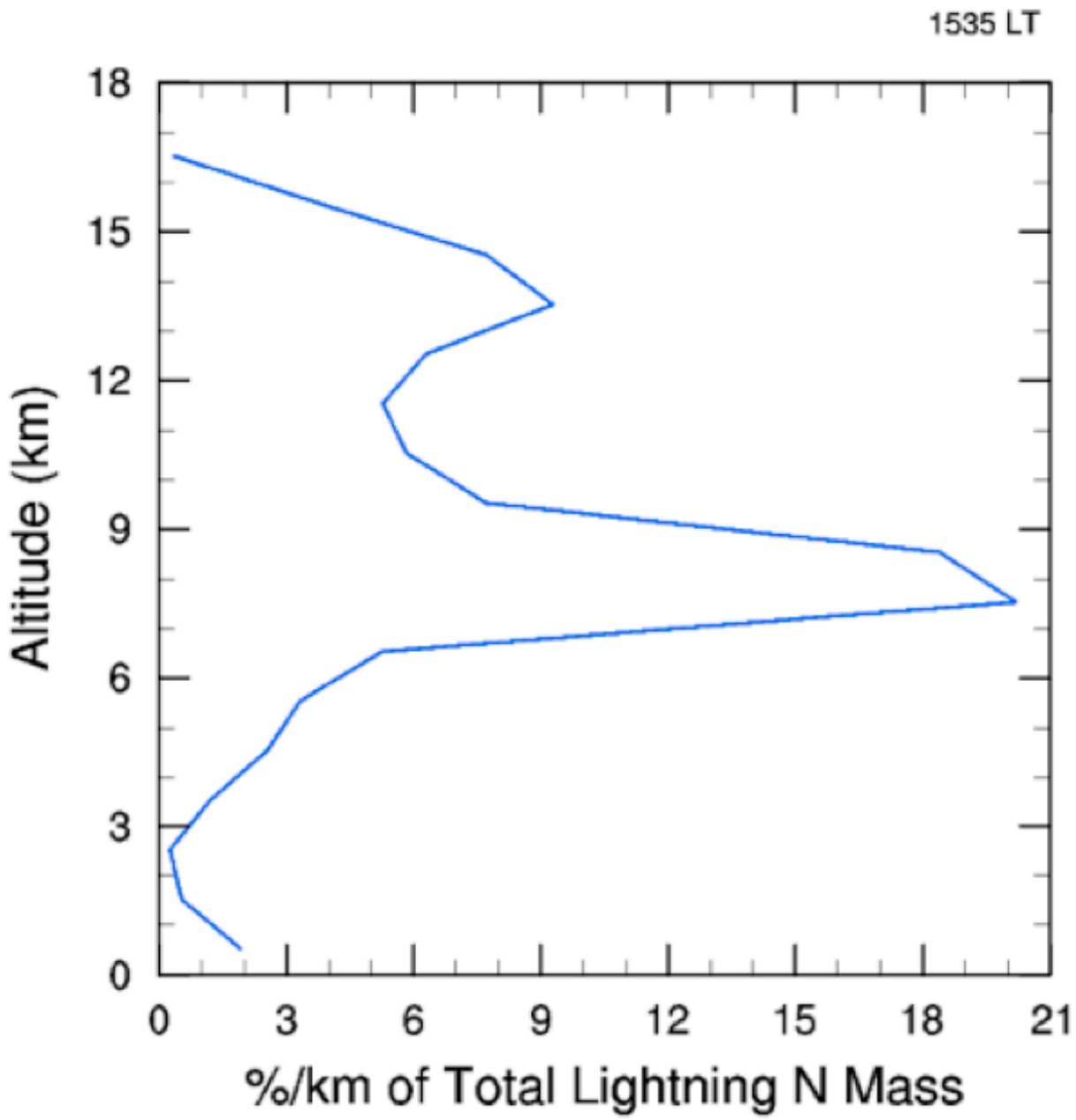

Figure 18. Vertical distribution of percentage of lightning NO_x mass per kilometer following convection at 15:35 LT given 500 moles NO flash^{-1}.

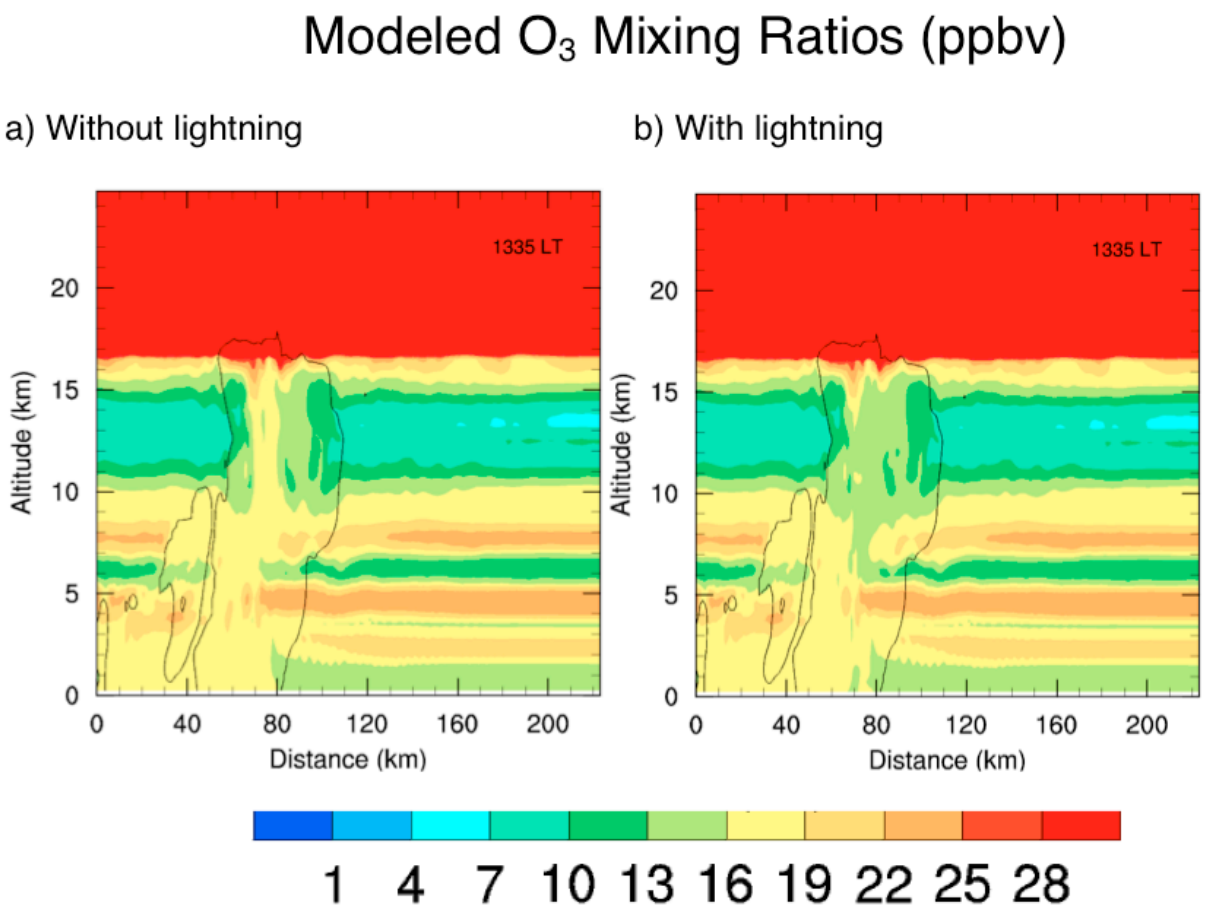

Figure 19. Vertical cross sections of O_3 mixing ratios, oriented 130º from north through the storm core, for simulations a) without and b) with lightning NO production. The cross sections occur during a peak in average NO_x production within the layers centered at 12.0 km and 12.7 km. The thin black line indicates the 0.01 g kg^{-1} total condensate contour.

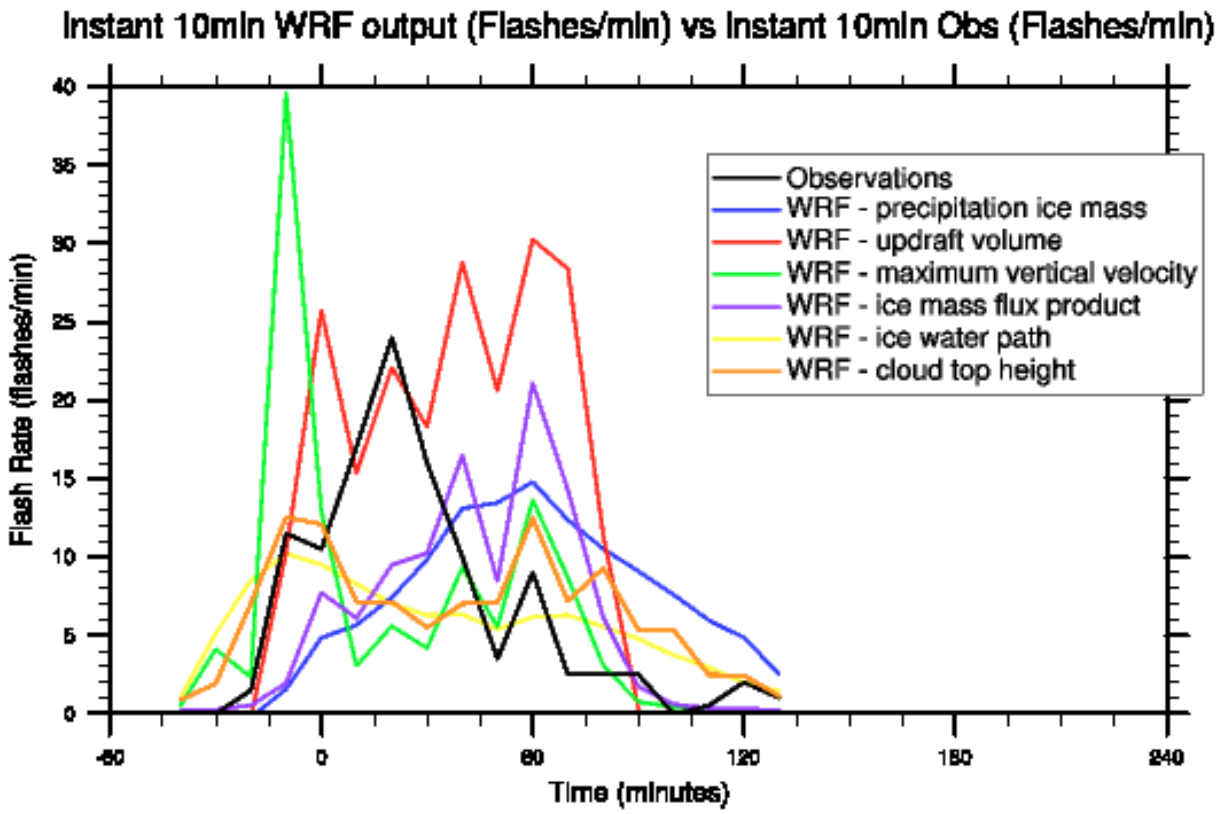

Figure 20. Total (IC and CG) flash rates based on instantaneous 10-minute interval observations and WRF model parameters. The observed flash rates trend overlays the six modeled trends, which are assumed to start at 12:35 LT. The x-axis represents 12:15-17:15 modeled time, where t=0 is 13:15 LT.

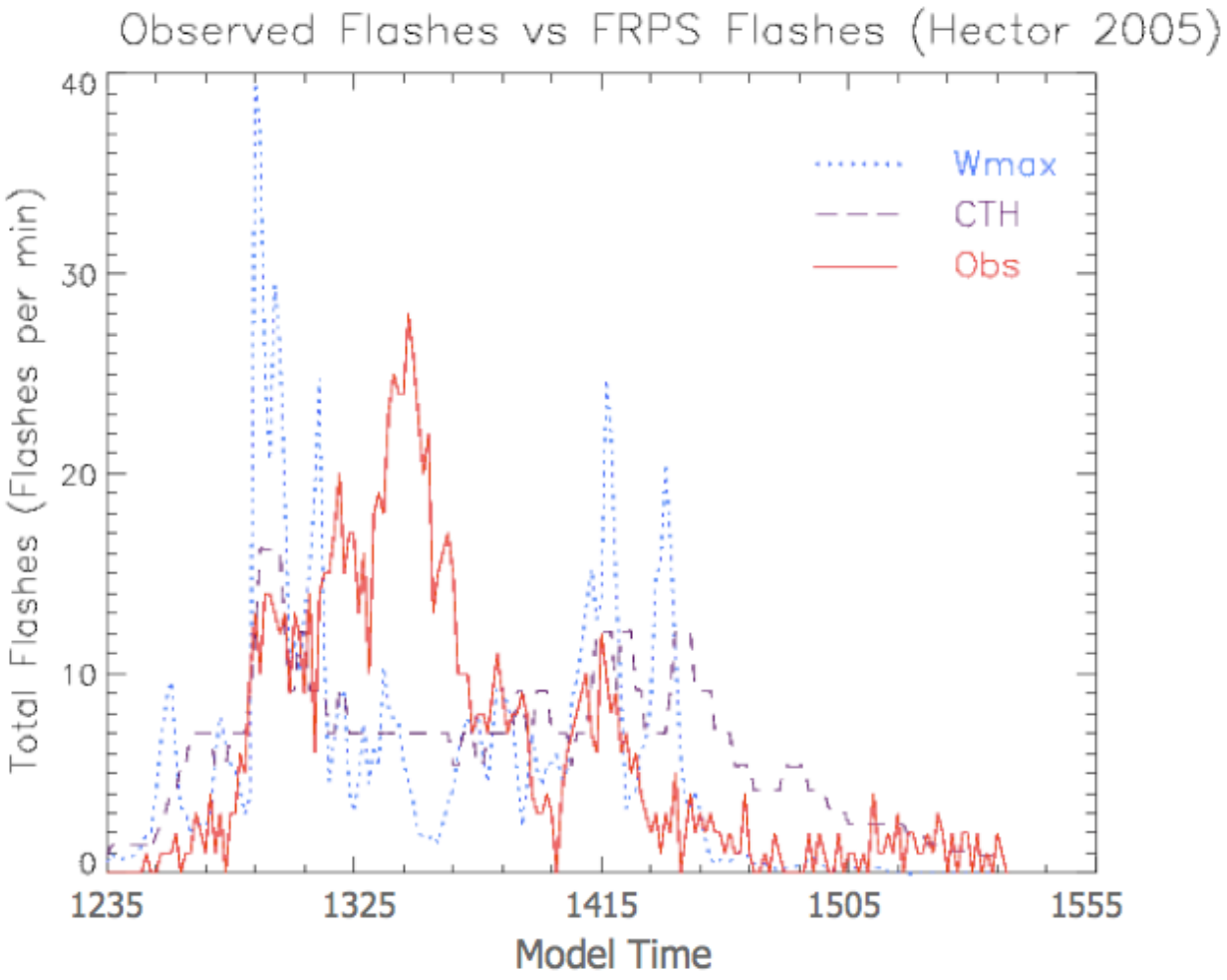

Figure 21. Observed and modeled total (IC and CG) flash rates per minute.

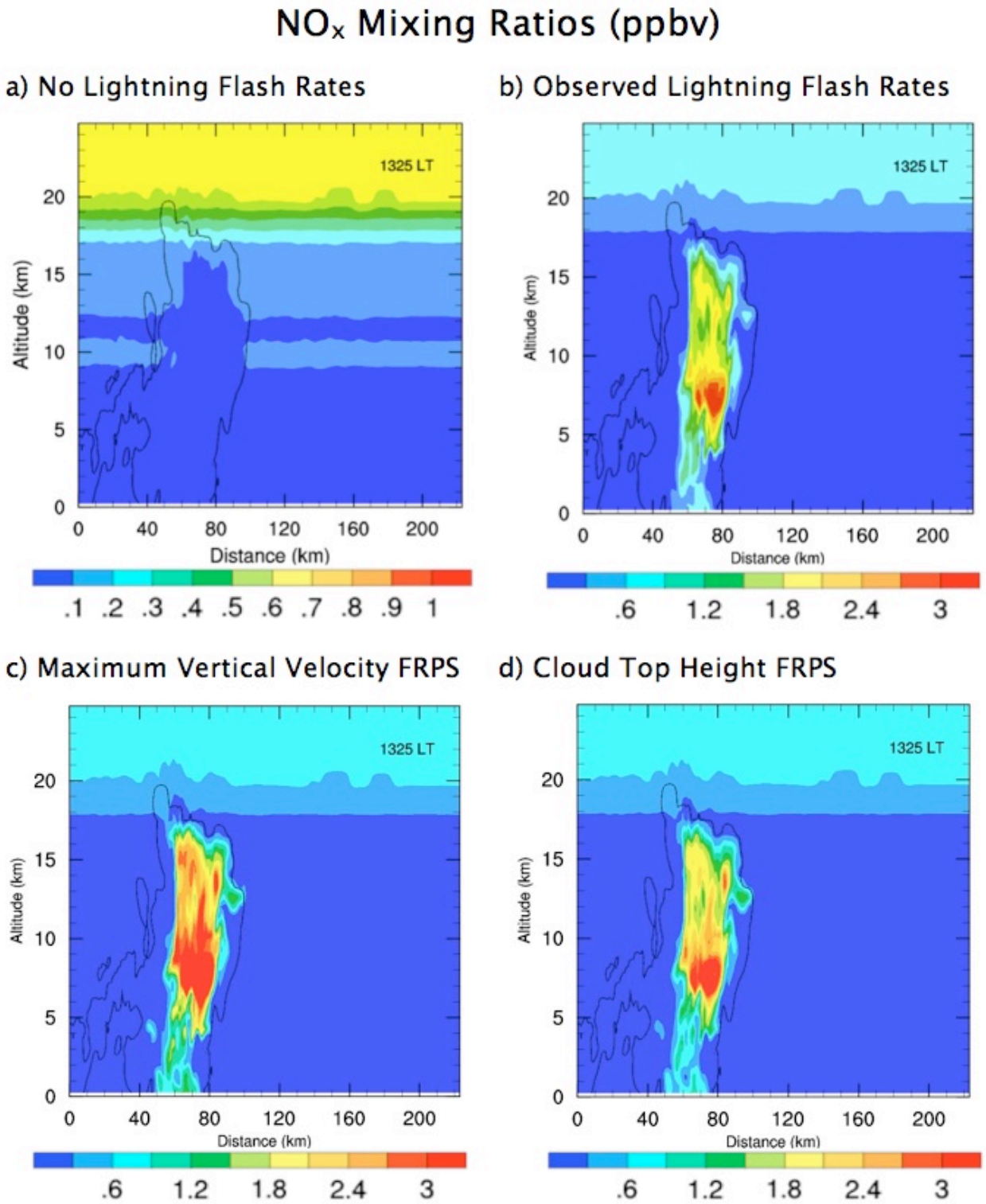

Figure 22. Vertical cross sections of NO_x mixing ratios, oriented 130º from north through the storm core, for simulations a) without and with lightning NO production of 500 moles flash^{-1} given b) observed flash rates, c) maximum vertical velocity FRPS, and d) cloud top height FRPS. The thin black line indicates the 0.01 g kg^{-1} total condensate contour.

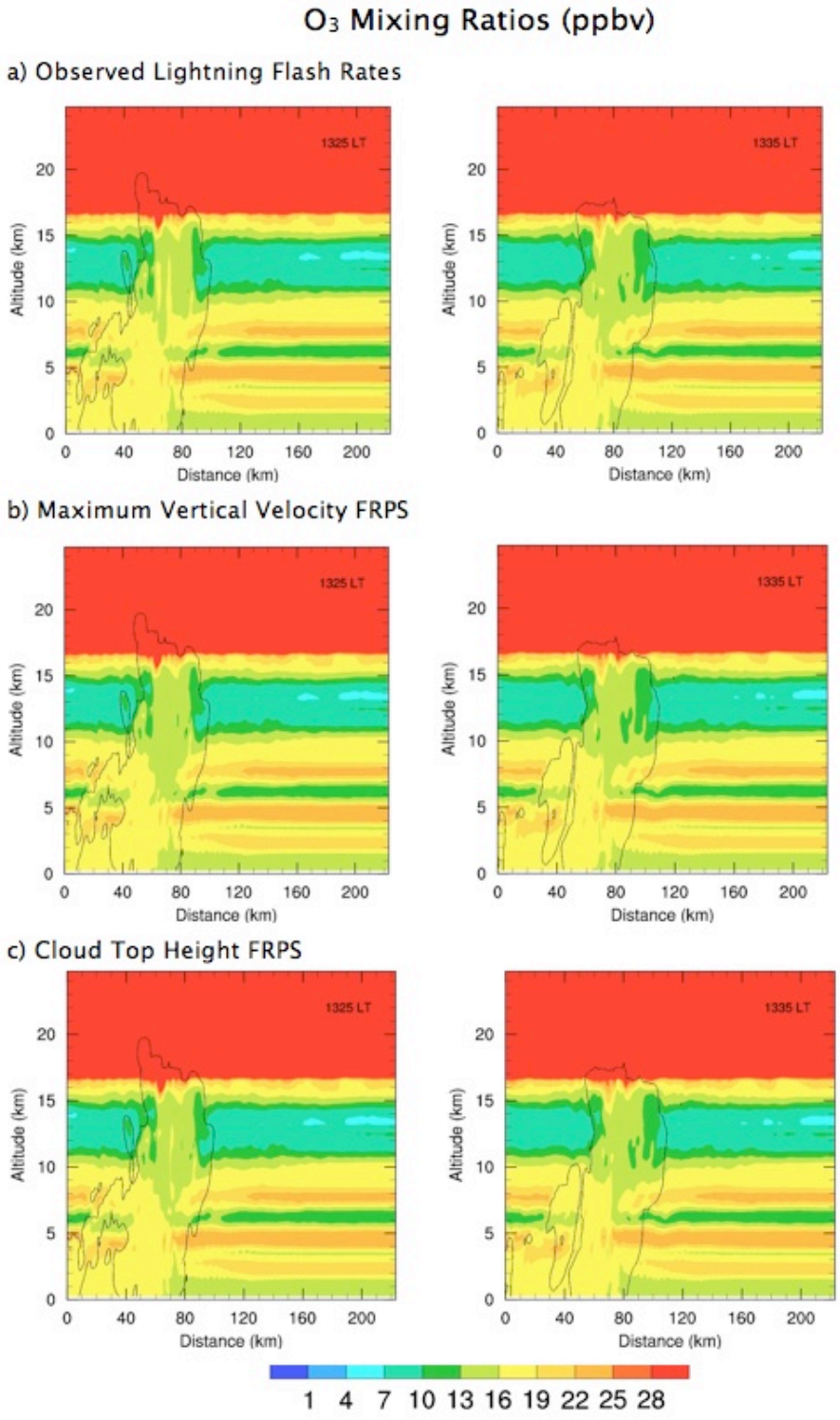

Figure 23. Vertical cross sections of O_3 mixing ratios, oriented 130º from north through the storm core, for simulations with lightning NO production of 500 moles flash^{-1} given a) observed flash rates, b) maximum vertical velocity FRPS, and c) cloud top height FRPS. The figures on the left and right represent O_3 distribution within the storm cloud at 13:25 LT and 13:35 LT, respectively. The thin black line indicates the 0.01 g kg^{-1} total condensate contour.